Data-driven discovery of Koopman eigenfunctions for control

IOP Publishing Mach. Learn.: Sci. Technol. 2 (2021) 035023 https://doi.org/10.1088/2632-2153/abf0f5

MACHINE LEARNING Science and Technology

CrossMark

OPEN ACCESS

RECEIVED
9 December 2020

REVISED
9 February 2021

ACCEPTED FOR PUBLICATION
22 March 2021

PUBLISHED
14 June 2021

PAPER

Data-driven discovery of Koopman eigenfunctions for control

Eurika Kaiser[1,*], J Nathan Kutz[2] and Steven L Brunton[1]

[1] Department of Mechanical Engineering, University of Washington, Seattle, WA 98195, United States of America
[2] Department of Applied Mathematics, University of Washington, Seattle, WA 98195, United States of America
[*] Author to whom any correspondence should be addressed.

E-mail: eurika@uw.edu

Keywords: dynamical systems, nonlinear control, Koopman theory, system identification, machine learning

Abstract

Data-driven transformations that reformulate nonlinear systems in a linear framework have the potential to enable the prediction, estimation, and control of strongly nonlinear dynamics using linear systems theory. The Koopman operator has emerged as a principled linear embedding of nonlinear dynamics, and its eigenfunctions establish intrinsic coordinates along which the dynamics behave linearly. Previous studies have used finite-dimensional approximations of the Koopman operator for model-predictive control approaches. In this work, we illustrate a fundamental closure issue of this approach and argue that it is beneficial to first validate eigenfunctions and then construct reduced-order models in these validated eigenfunctions. These coordinates form a Koopman-invariant subspace *by design* and, thus, have improved predictive power. We show then how the control can be formulated directly in these intrinsic coordinates and discuss potential benefits and caveats of this perspective. The resulting control architecture is termed *Koopman Reduced Order Nonlinear Identification and Control* (KRONIC). It is further demonstrated that these eigenfunctions can be approximated with data-driven regression and power series expansions, based on the partial differential equation governing the infinitesimal generator of the Koopman operator. Validating discovered eigenfunctions is crucial and we show that lightly damped eigenfunctions may be faithfully extracted from EDMD or an implicit formulation. These lightly damped eigenfunctions are particularly relevant for control, as they correspond to nearly conserved quantities that are associated with persistent dynamics, such as the Hamiltonian. KRONIC is then demonstrated on a number of relevant examples, including (a) a nonlinear system with a known linear embedding, (b) a variety of Hamiltonian systems, and (c) a high-dimensional double-gyre model for ocean mixing.

1. Introduction

In contrast to linear systems, a generally applicable and scalable framework for the control of nonlinear systems remains an engineering grand challenge. Improved nonlinear control has the potential to transform our ability to interact with and manipulate complex systems across broad scientific, technological, and industrial domains. From turbulence control to brain-machine interfaces, emerging technologies are characterized by high-dimensional, strongly nonlinear, and multiscale phenomena that lack simple models suitable for control design. This lack of simple equations motivates *data-driven* control methodologies, which include system identification for model discovery [9, 16, 22, 72, 85]. Alternatively, one can seek transformations that embed nonlinear dynamics in a global linear representation, as in the Koopman framework [63, 79]. The goal of this work is to reformulate controlled nonlinear dynamics in a Koopman-eigenfunction framework, referred to as *Koopman Reduced Order Nonlinear Identification and Control* (KRONIC), that shows improved predictive power and is amenable to powerful linear optimal and robust control techniques [36, 103, 106].

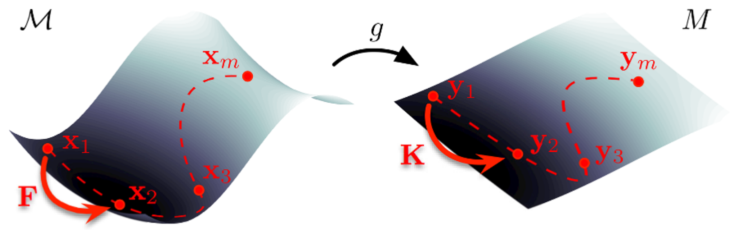

Figure 1. Koopman embedding to linearize nonlinear dynamics.

A wide range of data-driven and nonlinear control approaches exist in the literature, including model-free adaptive control [67], extremum-seeking [6], gain scheduling [97], feedback linearization [27], describing functions [115], sliding mode control [37], singular perturbation [62], geometric control [17], back-stepping [61], model predictive control [26, 78], reinforcement learning [110], and machine learning control [21, 47]. Although considerable progress has been made in the control of nonlinear systems [53, 67, 99], methods are generally tailored to a specific class of problems, require considerable mathematical and computational resources, or do not readily generalize to new applications. Currently there is no overarching framework for nonlinear control, that is generically applicable to a wide class of potentially high-dimensional systems, as exists for linear systems [36, 103]. Generally applicable frameworks, such as dynamic programming [15], Pontryagin's maximum principle [91], and model-predictive control (MPC) [2, 26], often suffer from the curse of dimensionality and require considerably computational effort, e.g. solving adjoint equations, when applied to nonlinear systems, which can be mitigated to some degree by combining these with low-dimensional, linear representations. Fortunately, the rise of big data, advances in machine learning, and new approaches in dynamical systems are changing how we approach these canonically challenging nonlinear control problems. For instance, recently deep reinforcement learning has been combined with MPC [90, 120], yielding impressive results in the large-data limit.

Koopman operator theory has recently emerged as a leading framework to obtain linear representations of nonlinear dynamical systems from data [79]. This operator-theoretic perspective complements the more standard geometric [45] and probabilistic [34, 35] perspectives. The ability to embed nonlinear dynamics in a linear framework (see figure 1) is particularly promising for the prediction, estimation, and control of nonlinear systems. In 1931, Koopman showed that a nonlinear dynamical system may be represented by an infinite-dimensional linear operator acting on the space of measurement functions of the state of the system [63]. Formulating dynamics in terms of measurements is appealing in the era of big data. Since the seminal work of Mezić and Banaszuk [84] and Mezić [79], Koopman theory has been the focus of efforts to characterize nonlinear systems. Many classical results have been extended to the Koopman formalism [25, 80]. For example, level sets of Koopman eigenfunctions form invariant partitions [24] and may be used to analyze mixing. The Hartman–Grobman theorem has also been generalized to provide a linearizing transform in the entire basin of attraction of a stable or unstable equilibrium or periodic orbit [71].

Recently, Koopman theory has been applied for system identification [75, 81, 93, 116], estimation [107, 108] and control [1, 20, 64, 105, 119] of nonlinear systems. The Koopman operator is infinite-dimensional, and control laws are typically based on a finite-dimensional approximation. Dynamic mode decomposition (DMD) [68, 96, 100, 114] approximates the Koopman operator with a best-fit linear model. However, DMD is based on linear measurements, which do not span a Koopman invariant subspace for many nonlinear systems [20, 68, 117]. Current data-driven methods to approximate the Koopman operator include extended DMD (EDMD) [59, 117, 118] and the variational approach of conformation dynamics (VAC) [86, 87]. EDMD was recently used for model predictive control with promising results [64]. However, EDMD models may suffer from closure issues for systems with multiple fixed points or attractors, as a linear model only has a single fixed point [20], which may lead to corrupted dynamics [20, 68] and emphasizes the importance of model validation. For instance, some eigenfunctions may be distorted when projected onto a finite-dimensional measurement subspace, and it may be advantageous to construct a reduced-order description from *validated* eigenfunctions, that exhibit behavior as predicted by their associated eigenvalue. For chaotic systems, delay coordinates provides a promising embedding [5, 19, 109]. Obtaining useful data-driven coordinate transformations that approximate Koopman eigenfunctions remains an open challenge in data-driven dynamical systems [20, 68].

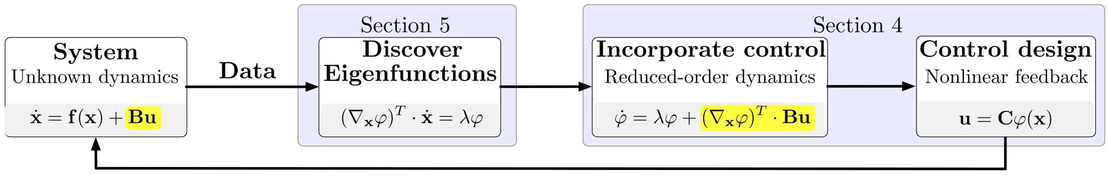

Figure 2. Control of nonlinear systems via reduced Koopman-invariant representations in eigenfunction coordinates.

In the present work, we build on the existing EDMD and reformulate the Koopman-based control problem in eigenfunction coordinates and provide strategies to identify lightly damped eigenfunctions from data, that can be subsequently used for control. In particular:

- Koopman eigenfunctions provide a principled linear embedding of nonlinear dynamics resulting in an intrinsic coordinate system, in which the system is closed under the action of the Koopman operator. We formulate the incorporation of control in these intrinsic coordinates and discuss benefits and caveats of this approach. Further, Koopman eigenfunctions can be associated with geometric system properties and coherent structures. Thus, the designed controller may be employed to manipulate particular coherent structures. For example, the Hamiltonian energy is a Koopman eigenfunction, and we are able to control the system by manipulating this function.
- Smooth eigenfunctions in the point spectrum of the Koopman operator can be discovered from given data using sparse regression providing interpretable representations. We propose sparsity-promoting algorithms to regularize EDMD or to discover eigenfunctions directly in an implicit formulation.
- We further demonstrate the importance of model validation to distinguish *accurately identified* eigenfunctions from *spurious* ones. Lightly damped eigenfunctions are often not corrupted and can be used to construct reduced-order Koopman models.

These nonlinear control techniques generalize to *any* lightly damped eigenfunction. As a more sophisticated example, we consider the double gyre flow, which is a model for ocean mixing. The discovery of intrinsic coordinates for optimized nonlinear control establishes our data-driven KRONIC framework[3], shown in figure 2.

The present work is outlined as follows: in section 2, we demonstrate the importance of eigenfunction validation and motivate the use of sparse regression for their discovery. In section 3, key results in Koopman spectral theory and corresponding data-driven approaches are summarized, and a brief background on optimal control is provided. The approach for identifying of Koopman eigenfunctions from data using sparse regression is outlined in section 5. In section 4, it is shown how control can be incorporated in the eigenfunction formulation. An analytical example is examined in section 6 to illustrate the control problem in terms of Koopman eigenfunction coordinates. The KRONIC framework is then demonstrated on several Hamiltonian systems (section 7), for basin-hopping in an asymmetric double potential well (section 8), and the autonomous and non-autonomous double gyre flow (section 9). A discussion and outlook on future directions is provided in section 10.

2. Motivation

Finite-dimensional approximations of the Koopman operator are typically obtained as its projection onto a specified basis or dictionary. EDMD [116] has emerged as the leading numerical approach by solving a least-squares problem. A well-known issue arises when trying to identify the full operator in a finite set of basis functions, that sometimes the finite-dimensional approximation is not closed and spurious eigenfunctions may appear. For this reason, it can be important to perform consistency checks, such as validating the linearity property of eigenfunctions. The present work builds on EDMD addressing this limitation by re-formulating the regression problem for the direct identification of Koopman eigenfunctions. Further, we demonstrate how EDMD may be regularized to obtain more accurate eigenfunction representations. In the following, we illustrate the closure problem using a polynomial basis. As a motivating example (examined in detail in section 6), we consider a system with quadratic nonlinearity that gives rise to

[3] Code at https://github.com/eurika-kaiser/KRONIC.

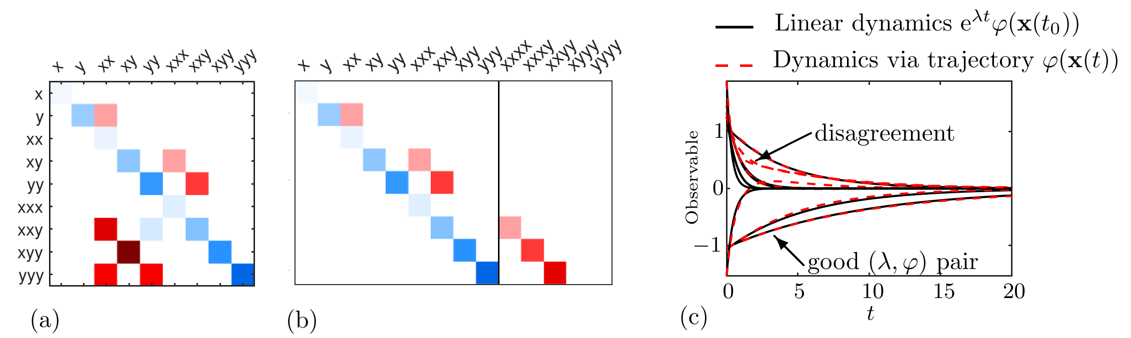

Figure 3. EDMD models give rise to inaccurate eigenvectors, demonstrated for the slow manifold system: (a) EDMD regression model on up to third degree monomials, (b) fitting onto higher-degree monomials, (c) evolution of eigenvectors identified from the model in (a), which are evaluated on a single test trajectory, and as predicted using the corresponding eigenvalue.

a slow manifold [114]:

$$\frac{\mathrm{d}}{\mathrm{d}t}\begin{bmatrix} x_1 \\ x_2 \end{bmatrix} = \begin{bmatrix} \mu x_1 \\ \lambda(x_2 - x_1^2) \end{bmatrix} \tag{1}$$

with $\mu = -0.1$ and $\lambda = -1$. By a clever choice of observable functions $\mathbf{y}$, the nonlinear system (1) may be represented as a linear system:

$$\frac{\mathrm{d}}{\mathrm{d}t}\mathbf{y} = \mathbf{K}\mathbf{y}, \tag{2}$$

where $\mathbf{K}$ represents a finite-dimensional approximation of the Koopman operator. The system (1) is one of few analytical examples, for which a closed, finite-dimensional, linear Koopman approximation exists.

The EDMD model fit on the first nine monomials (up to third degree) is shown in figure 3(a). Some of the eigenvectors are *spurious* (see figure 3(c)), i.e. the evolution of the eigenfunction $\varphi(\mathbf{x}(t))$ obtained by evaluating the eigenfunction on a trajectory $\mathbf{x}(t)$ does not correspond to the linear prediction using the eigenvalue, $e^{\lambda t}\varphi(\mathbf{x}(t_0))$. The reason is that the model is not closed in the particular choice of basis functions, because the derivatives of third degree monomials give rise to higher-degree monomials (see figure 3(b)) resulting in a nonlinear model:

$$\frac{\mathrm{d}}{\mathrm{d}t}\begin{bmatrix} y_1 \\ y_2 \\ y_3 \\ y_4 \\ y_5 \\ y_6 \\ y_7 \\ y_8 \\ y_9 \end{bmatrix} = \begin{bmatrix} \mu & 0 & 0 & 0 & 0 & 0 & 0 & 0 & 0 \\ 0 & \lambda & -\lambda & 0 & 0 & 0 & 0 & 0 & 0 \\ 0 & 0 & 2\mu & 0 & 0 & 0 & 0 & 0 & 0 \\ 0 & 0 & 0 & \mu+\lambda & -\lambda & 0 & 0 & 0 & 0 \\ 0 & 0 & 0 & 0 & 2\lambda & 0 & -2\lambda & 0 & 0 \\ 0 & 0 & 0 & 0 & 0 & 3\mu & 0 & 0 & 0 \\ 0 & 0 & 0 & 0 & 0 & 0 & \lambda+2\mu & 0 & 0 \\ 0 & 0 & 0 & 0 & 0 & 0 & 0 & 2\lambda+\mu & 0 \\ 0 & 0 & 0 & 0 & 0 & 0 & 0 & 0 & 3\lambda \end{bmatrix}\begin{bmatrix} y_1 \\ y_2 \\ y_3 \\ y_4 \\ y_5 \\ y_6 \\ y_7 \\ y_8 \\ y_9 \end{bmatrix} + \begin{bmatrix} 0 \\ 0 \\ 0 \\ 0 \\ 0 \\ 0 \\ -\lambda x_1^4 \\ -2\lambda x_1^3 x_2 \\ -3\lambda x_1^2 x_2^2 \end{bmatrix}, \tag{3}$$

where $(y_1, y_2, y_3, y_4, y_5, y_6, y_7, y_8, y_9) = (x_1, x_2, x_1^2, x_1x_2, x_2^2, x_1^3, x_1^2x_2, x_1x_2^2, x_3^3)$. These additional terms, that are not in the span of $\{y_1, \ldots, y_9\}$, will be *aliased* in the corresponding row equations corrupting the system matrix $\mathbf{K}$. Thus, some of the eigenfunctions will be spurious, affecting the prediction accuracy of the model based on $\mathbf{K}$. However, it may be possible to identify a subset of the eigenfunctions that are not corrupted, e.g. those eigenpairs that show good agreement in figure 3(c), and use these to construct a reduced-order model with improved prediction. Alternatively, EDMD may be regularized using sparsity-promoting techniques to regress a (approximate) closed model on a subset of basis functions. For instance, choosing the five observable functions $(y_1, y_2, y_3, y_4, y_5) = (x_1, x_2, x_1^2, x_1x_2, x_1^3)$, which are a subset of the nine monomials used above, yields:

$$\frac{\mathrm{d}}{\mathrm{d}t}\begin{bmatrix} y_1 \\ y_2 \\ y_3 \\ y_4 \\ y_5 \end{bmatrix} = \begin{bmatrix} \mu & 0 & 0 & 0 & 0 \\ 0 & \lambda & -\lambda & 0 & 0 \\ 0 & 0 & 2\mu & 0 & 0 \\ 0 & 0 & 0 & \mu+\lambda & -\lambda \\ 0 & 0 & 0 & 0 & 3\mu \end{bmatrix}\begin{bmatrix} y_1 \\ y_2 \\ y_3 \\ y_4 \\ y_5 \end{bmatrix}, \tag{4}$$

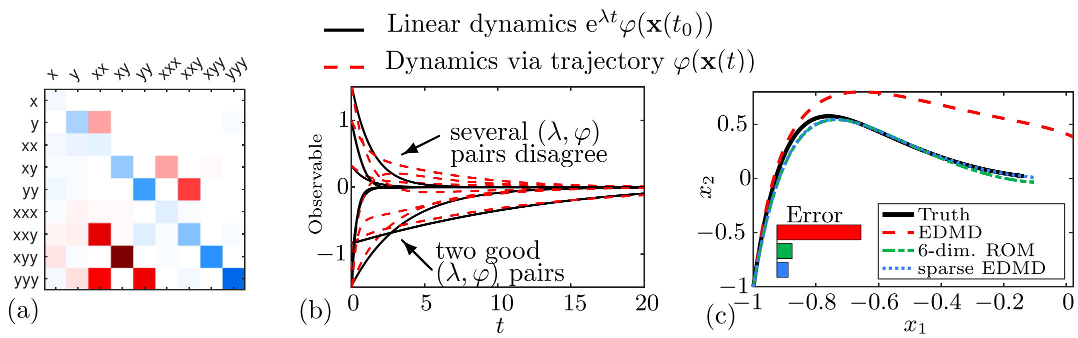

Figure 4. Sparsified EDMD models increase robustness and prevent overfitting on noisy data: (a) EDMD model, (b) validation of eigenpairs, and (c) phase plot with L_2 error for different models. For details see figure 3 and text.

which is a 5-dim. linear system, that remains closed under the action of the Koopman operator.

Measurements from real-world systems are generally corrupted by noise, which can be more challenging for model identification procedures. Figure 4(c) shows the poor prediction performance of the EDMD model trained on noisy data (displayed in figure 4(a)). More eigenfunctions are inaccurate as a result of an increasing number of non-vanishing coefficients in the state matrix compared with the noise-free situation in figure 3. The least-squares solution overfits resulting in a full matrix with small, but non-vanishing coefficients. By sparsifying the EDMD state matrix or constructing a reduced-order model based on accurate eigenfunctions (validated from figure 4(b)) higher prediction accuracy and robustness to noise can be achieved (compare models in figure 4(c)). Ideally, it would be possible to learn *good* eigenfunctions directly, which are designed to behave linearly and evolve as predicted by their associated eigenvalue, which would potentially significantly increase prediction accuracy and reduce the dimension of the model.

3. Background

In this section, we provide a brief background on Koopman spectral theory in section 3.1 and a numerical algorithm, dynamic mode decomposition, to approximate the Koopman operator in section 3.2. Key results in optimal control are then summarized in section 3.3.

3.1. Koopman spectral theory

The classical geometric theory of dynamical systems considers a set of coupled ordinary differential equations

$$\frac{\mathrm{d}}{\mathrm{d}t}\mathbf{x}(t) = \boldsymbol{f}(\mathbf{x}) \tag{5}$$

in terms of the state of the system $\mathbf{x} \in \mathcal{M}$, where $\mathcal{M}$ is a differentiable manifold, often given by $\mathcal{M} = \mathbb{R}^n$. In discrete time, the dynamics are given by

$$\mathbf{x}_{k+1} = \mathbf{F}(\mathbf{x}_k), \tag{6}$$

where $\mathbf{F}$ may be the flow map of the dynamics in (5):

$$\mathbf{F}(\mathbf{x}(t_0)) = \mathbf{x}(t_0) + \int_{t_0}^{t_0+t} \boldsymbol{f}(\mathbf{x}(\tau))\,\mathrm{d}\tau. \tag{7}$$

Discrete-time systems are more general and form a superset, containing those induced by continuous-time dynamics. Moreover, discrete-time dynamics are often more consistent with experimental measurements, and may be preferred for numerical analysis. The geometric perspective then considers fixed points and invariant structures of the dynamics.

In 1931, Koopman introduced the operator theoretic perspective, showing that there exists an infinite-dimensional linear operator, given by $\mathcal{K}$, that acts to advance all measurement functions $g : \mathcal{M} \to \mathbb{R}$ of the state with the flow of the dynamics:

$$\mathcal{K}g = g \circ \mathbf{F}. \tag{8}$$

Thus, the Koopman operator advances measurements linearly:

$$g(\mathbf{x}_{k+1}) = \mathcal{K}g(\mathbf{x}_k). \tag{9}$$

For smooth dynamics, there is a continuous system

$$\frac{\mathrm{d}}{\mathrm{d}t} g(\mathbf{x}) = \mathcal{K} g(\mathbf{x}) = \nabla g(\mathbf{x}) \cdot \mathbf{f}(\mathbf{x}), \tag{10}$$

where $\mathcal{K}$ is the infinitesimal generator of the one-parameter family of Koopman operators K.

The Koopman operator is linear, which is appealing, but is infinite dimensional, posing issues for representation and computation. Instead of capturing the evolution of all measurement functions in a Hilbert space, applied Koopman analysis approximates the evolution on a subspace spanned by a finite set of measurement functions. It is possible to obtain a finite-dimensional matrix representation of the Koopman operator by restricting it to an invariant subspace. A Koopman invariant subspace is spanned by any set of eigenfunctions of the Koopman operator. A Koopman eigenfunction $\varphi(\mathbf{x})$ corresponding to eigenvalue λ satisfies

$$\lambda \varphi(\mathbf{x}) = \varphi(\mathbf{F}(\mathbf{x})). \tag{11}$$

In continuous-time, a Koopman eigenfunction $\varphi(\mathbf{x}) : \mathcal{M} \to \mathbb{C}$ satisfies

$$\frac{\mathrm{d}}{\mathrm{d}t} \varphi(\mathbf{x}) = \lambda \varphi(\mathbf{x}). \tag{12}$$

Obtaining Koopman eigenfunctions from data or analytically is a central applied challenge in modern dynamical systems. Discovering these eigenfunctions enables globally linear representations of strongly nonlinear systems in terms of these *intrinsic* observables. The evolution equation (12) describes the unactuated behavior, which will be extended to incorporate the effect of control in our KRONIC framework (compare the third box in figure 2 and for further details we refer to sections 4 and 5).

3.2. Dynamic mode decomposition

Dynamic mode decomposition (DMD) is a simple numerical algorithm that approximates the Koopman operator with a best-fit linear model that advances measurements from one time step to the next [68, 96, 100, 114]. DMD was originally introduced in the fluid dynamics community [8, 21, 43, 80, 100, 101] to decompose large data sets into dominant spatial-temporal coherent structures, and a connection with Koopman theory was soon established [96]. In addition to fluid dynamics, DMD has been widely applied to a range of problems in neuroscience [18], robotics [14], epidemiology [94], and video processing [40, 44, 70]. The DMD algorithm has also been extended to include sparsity and compressed sensing [23, 40, 46, 55, 113], actuation and control [92], multi-resolution analysis [69], de-noising [33, 50], and streaming variants [51].

In DMD, the infinite-dimensional Koopman operator in (9) is approximated with a finite-dimensional matrix $\mathbf{A}$ that advances the system state $\mathbf{x}$:

$$\mathbf{x}_{k+1} \approx \mathbf{A}\mathbf{x}_k. \tag{13}$$

Given data from a nonlinear system in (6), it is possible to stack snapshots into a matrix $\mathbf{X} = [\mathbf{x}_1\ \mathbf{x}_2\ \dots\ \mathbf{x}_{m-1}]$ and a time-shifted matrix $\mathbf{X}' = [\mathbf{x}_2\ \mathbf{x}_3\ \dots\ \mathbf{x}_m]$. In terms of these data matrices, (13) becomes

$$\mathbf{X}' \approx \mathbf{A}\mathbf{X}. \tag{14}$$

Various DMD algorithms then compute the leading eigendecomposition of the best-fit linear operator $\mathbf{A}$, given by

$$\mathbf{A} = \arg\min_{\widetilde{\mathbf{A}}} ||\mathbf{X}' - \widetilde{\mathbf{A}}\mathbf{X}||_F, \tag{15}$$

where $\|\cdot\|_F$ is the Frobenius norm. The best-fit $\mathbf{A}$ is given by $\mathbf{A} = \mathbf{X}'\mathbf{X}^\dagger$, where $\dagger$ is the pseudo-inverse, which is computed via singular value decomposition.

DMD has proven to be an extremely useful technique for the analysis of high-dimensional dynamical systems data. However, DMD is based on linear measurements of the system, which do not typically span a Koopman-invariant subspace of a general nonlinear system. For example, a linear DMD model may perfectly capture the periodic attractor dynamics of a system on a limit cycle, but will fail to capture the nonlinear transients if the system is perturbed off the attractor. DMD has since been augmented with nonlinear measurements to enrich the model in EDMD [59, 117, 118] and VAC [86, 87]. EDMD models have been used with success for estimation [107, 108] and model predictive control [64]. However, EDMD models are based on a large set of nonlinear measurements of the state, and there is no guarantee that these measurements form a Koopman invariant subspace. In fact, EDMD measurement subspaces will generally *not* be closed [20, 68]. For example, there is no finite-dimensional Koopman invariant subspace that includes the state of the system $\mathbf{x}$ for any dynamical system that has multiple attractors (e.g. fixed points, periodic orbits, etc), since the resulting finite-dimensional linear model cannot be topologically conjugate to the original dynamics. This is closely related to the representation of the Koopman operator in a polynomial basis, similar to Carleman linearization [10, 66, 111]. Thus, EDMD as well as other models are often plagued with spurious eigenfunctions that do not behave linearly as predicted by the associated eigenvalue. Fortunately, although these models may have corrupted eigenvalues and eigenfunctions, eigenfunctions corresponding to lightly damped eigenvalues may be faithfully extracted.

3.3. Optimal control

The overarching goal of Koopman control is to reformulate strongly nonlinear dynamics in a linear framework to enable the use of powerful optimal and robust control techniques available for linear systems [36, 103, 106]. Here, we summarize key results in optimal control theory that will be used for control in Koopman eigenfunction coordinates. We consider the nonlinear system (5) affected by an external input

$$\frac{\mathrm{d}}{\mathrm{d}t}\mathbf{x}(t) = \boldsymbol{f}(\mathbf{x},\mathbf{u}), \quad \mathbf{x}(0) = \mathbf{x}_0 \tag{16}$$

with multi-channel control input $\mathbf{u} \in \mathbb{R}^q$ and continuously differentiable dynamics $\boldsymbol{f}(\mathbf{x},\mathbf{u}) : \mathbb{R}^n \times \mathbb{R}^q \to \mathbb{R}^n$. Without loss of generality, the origin is an equilibrium: $\boldsymbol{f}(\mathbf{0},\mathbf{0}) = \mathbf{0}$.

Infinite-horizon optimal control minimizes the following quadratic cost functional

$$J(\mathbf{x},\mathbf{u}) = \frac{1}{2}\int_0^\infty \underbrace{\mathbf{x}^T(t)\mathbf{Q}\mathbf{x}(t) + \mathbf{u}^T(t)\mathbf{R}\mathbf{u}(t)}_{L(\mathbf{x},\mathbf{u})}\,\mathrm{d}t \tag{17}$$

with state and input weight matrices $\mathbf{Q} \in \mathbb{R}^{n\times n}$ and $\mathbf{R} \in \mathbb{R}^{q\times q}$. Both matrices are symmetric and fulfill $\mathbf{Q} > 0$ and $\mathbf{R} \geqslant 0$. A full-state feedback control law

$$\mathbf{u}(\mathbf{x}) = -\mathbf{C}(\mathbf{x})\mathbf{x} = \mathbf{c}(\mathbf{x}), \quad \mathbf{c}(\mathbf{0}) = \mathbf{0} \tag{18}$$

with gain $\mathbf{C} : \mathbb{R}^n \to \mathbb{R}^{q\times n}$ is sought that minimizes the cost function (17) subject to the state dynamics (16) to drive the system to the origin, i.e. $\lim_{t\to\infty} \mathbf{x}(t) = \mathbf{0}, \forall \mathbf{x}$.

4. Koopman operator control in eigenfunctions

We now propose a general control architecture in Koopman eigenfunction coordinates, referred to as KRONIC (see figure 2). This eigenfunction perspective relies on a model constructed from validated Koopman eigenfunctions, which is closed and linear by design. First, we derive how the effect of actuation affects the dynamics of these eigenfunction coordinates. Second, the optimal control problem is formulated in these coordinates and a corresponding feedback controller is then developed, yielding a possibly nonlinear control law in the original state variables. Control in eigenfunction coordinates is quite general, encompassing the stabilization of fixed points and periodic orbits, e.g. via the Hamiltonian eigenfunction, or the manipulation of more general spatial-temporal coherent structures given by level sets of other eigenfunctions.

4.1. Control–affine systems

We first examine how adding control to a dynamical system (5) affects a single Koopman eigenfunction. This formulation then readily generalizes to multiple eigenfunctions. Consider a control-affine system

$$\frac{\mathrm{d}}{\mathrm{d}t}\mathbf{x}(t) = \boldsymbol{f}(\mathbf{x}) + \sum_{i=1}^{q}\mathbf{b}_i(\mathbf{x})u_i, \tag{19}$$

with a multi-channel input $\mathbf{u} \in \mathbb{R}^q$, continuously differentiable dynamics $\boldsymbol{f}(\mathbf{x}) : \mathbb{R}^n \to \mathbb{R}^n$ associated with the unforced dynamics, and each $\mathbf{b}_i(\mathbf{x})$ is a vector field acting on the state space.

Starting with the Koopman operator associated with the uncontrolled, autonomous system (see section 3.1), we examine how the control terms in (19) affect the dynamics of its eigenfunctions. By applying the chain rule, we obtain

$$\frac{\mathrm{d}}{\mathrm{d}t}\varphi(\mathbf{x}) = \nabla\varphi(\mathbf{x})\cdot\left(\boldsymbol{f}(\mathbf{x}) + \sum_{i=1}^{q}\mathbf{b}_i(\mathbf{x})u_i\right) \tag{20a}$$

$$= \lambda\varphi(\mathbf{x}) + \nabla\varphi(\mathbf{x})\cdot\sum_{i=1}^{q}\mathbf{b}_i(\mathbf{x})u_i. \tag{20b}$$

This equation differs from equation (12) in the additional second term associated with the control terms. The $\varphi(\mathbf{x})$ is a Koopman eigenfunction associated with the autonomous Koopman operator for the unforced dynamics $\mathbf{f}(\mathbf{x})$. For instance, a Hilbert space of the Lebesque square-integrable functions may be considered as function space. The control enters the dynamics of φ via the additional term leading to a control-affine system, which is linear in φ and possibly nonlinear in the control.

Without loss of generality, we assume in the examples presented in later sections a linear control term:

$$\frac{\mathrm{d}}{\mathrm{d}t}\mathbf{x}(t) = \boldsymbol{f}(\mathbf{x}) + \mathbf{B}\mathbf{u}, \tag{21}$$

with control matrix $\mathbf{B}\in\mathbb{R}^{n\times q}$, so that the dynamics of the eigenfunctions become

$$\frac{\mathrm{d}}{\mathrm{d}t}\varphi(\mathbf{x}) = \lambda\varphi(\mathbf{x}) + \nabla\varphi(\mathbf{x})\cdot\mathbf{B}\mathbf{u}. \tag{22a}$$

4.2. Nonaffine control systems

More generally, we may be interested in the control of a nonlinear, non-affine system:

$$\frac{\mathrm{d}}{\mathrm{d}t}\mathbf{x}(t) = \boldsymbol{f}(\mathbf{x},\mathbf{u}), \tag{23}$$

with continuously differentiable dynamics $\boldsymbol{f}(\mathbf{x},\mathbf{u}):\mathbb{R}^n\times\mathbb{R}^q\to\mathbb{R}^n$. We may now consider an observable $g(\mathbf{x},\mathbf{u})$ as a function of the extended state space $\mathcal{M}\times\mathcal{U}$, where $\mathbf{x}\in\mathcal{M}$ and $\mathbf{u}\in\mathcal{U}$, and the non-autonomous Koopman operator acting on these observables. For discrete-time dynamics with discrete map $\mathbf{F}(\mathbf{x},\mathbf{u})$, the Koopman operator propagates scalar measurements according to $Kg(\mathbf{x}_k,\mathbf{u}_k) = g(\mathbf{F}(\mathbf{x}_k,\mathbf{u}_k),\mathbf{u}_{k+1})$ by assuming the Koopman operator acts on the extended state space in the same manner as the Koopman operator associated with the autonomous, unforced system. This assumption has been previously [64] considered, where the extended space was defined as the product of the original state-space and the space of all control sequences. Since the first appearance of this article, they have been further studies [4, 56, 93] examining the approximation of the Koopman operator for the non-affine control system. In [93], it is in more detail discussed how the Koopman operator formulation can be modified based on the dynamics of $\mathbf{u}$ itself, e.g. open-loop versus closed-loop control. As associated function space, in which observables are defined on the extended state space, a Hilbert space of the Lebesque square-integrable functions or polynomial functions defined on a compact set may be considered. If the dynamics on $\mathbf{u}$ are governed by a specific feedback law of the form $\mathbf{u} = \mathbf{C}(\mathbf{x})$, that is only a function of the state $\mathbf{x}$, then choices about the function space for the controlled system are equivalent to those applying to the autonomous system.

For smooth dynamics (23), the continuous-time dynamics are given by

$$\frac{\mathrm{d}}{\mathrm{d}t}g(\mathbf{x},\mathbf{u}) = \mathcal{K}g(\mathbf{x},\mathbf{u}). \tag{24}$$

An associated Koopman eigenfunction $\varphi(\mathbf{x},\mathbf{u})$ satisfies

$$\frac{\mathrm{d}}{\mathrm{d}t}\varphi(\mathbf{x},\mathbf{u}) = \lambda\varphi(\mathbf{x},\mathbf{u}). \tag{25}$$

Applying the chain rule, we find that the dynamics of the Koopman eigenfunction depends on $\dot{\mathbf{u}}$, which is generally arbitrary: $\frac{\mathrm{d}}{\mathrm{d}t}\varphi(\mathbf{x},\mathbf{u}) = \nabla_{\mathbf{x}}\varphi(\mathbf{x},\mathbf{u})\cdot\mathbf{f}(\mathbf{x},\mathbf{u}) + \nabla_{\mathbf{u}}\varphi(\mathbf{x},\mathbf{u})\cdot\dot{\mathbf{u}}$. Instead, we may specify that $\varphi(\mathbf{x},\mathbf{u})$ reduces to the eigenfunction $\varphi(\mathbf{x},\bar{\mathbf{u}})$ of $\dot{\mathbf{x}} = \boldsymbol{f}(\mathbf{x},\bar{\mathbf{u}})$ for all locked $\bar{\mathbf{u}}\in\mathcal{U}$, as in [93]. In this case, the eigenfunction is *parametrized* by the input $\bar{\mathbf{u}}$:

$$\nabla_{\mathbf{x}}\varphi(\mathbf{x},\bar{\mathbf{u}})\cdot\boldsymbol{f}(\mathbf{x},\bar{\mathbf{u}}) = \lambda\varphi(\mathbf{x},\bar{\mathbf{u}}),\quad\forall\,\bar{\mathbf{u}}\in\mathcal{U}. \tag{26}$$

These are eigenfunctions of the parametrized Koopman generator, which is autonomous for each locked $\bar{\mathbf{u}}$ and can be defined on the commonly used function spaces as stated above. This perspective is also assumed within the gEDMD framework and its extension for control [60]. The Koopman generator $\mathcal{K}$ is approximated as a finite-rank matrix $\mathbf{K}$ parametrized by the discrete control input using EDMD. The control problem is then solved by optimizing switching times among the finite set of discrete control inputs and associated models.

If we augment the eigenfunction vector with the input $\mathbf{u}$, we obtain

$$\frac{\mathrm{d}}{\mathrm{d}t}\varphi(\mathbf{x},\mathbf{u}) = \lambda\varphi(\mathbf{x},\mathbf{u}) + \nabla_{\mathbf{u}}\varphi(\mathbf{x},\mathbf{u})\cdot\dot{\mathbf{u}}, \tag{27}$$

where we view $\dot{\mathbf{u}}$ as the input to the Koopman linear system, and the $\nabla_{\mathbf{u}}\varphi(\mathbf{x},\mathbf{u})$ matrix varies based on $\mathbf{x}$ and $\mathbf{u}$. Thus, we may enact a gain-scheduled control law.

Summarizing, if the original dynamics are nonlinear and control-affine, the dynamics in Koopman eigenfunction coordinates are control-affine and split into a linear part associated with the nonlinear unforced dynamics and a bilinear part associated with the control term. If the original dynamics are nonlinear and non-affine in the control, the eigenfunction dynamics can become linear if the Koopman operator is defined on the extended state. Considering practical implications, it is also possible to modify these dynamics so that these consist of a linear part and a bilinear control term as in equation (27). We also point out, that while the control is generally nonlinear in the state $\mathbf{x}$, it may become linear in the eigenfunction coordinates for special cases, such as $\nabla\varphi(\mathbf{x}) = \mathrm{const.}$

4.3. Formulation of the optimal control problem

We now formulate the infinite-horizon, optimal control problem [106] for a reduced set of Koopman eigenfunctions. The control objective is a quadratic cost functional:

$$J(\boldsymbol{\varphi},\mathbf{u}) = \frac{1}{2}\int_0^\infty \boldsymbol{\varphi}^T(\mathbf{x}(t))\mathbf{Q}_\varphi\boldsymbol{\varphi}(\mathbf{x}(t)) + \mathbf{u}^T(t)\mathbf{R}\mathbf{u}(t)\,\mathrm{d}t, \tag{28}$$

where $\boldsymbol{\varphi} = [\varphi_1\,\varphi_2\,\ldots\,\varphi_r]^T$ comprises r eigenfunctions with φ_j associated with eigenvalue λ_j. For this cost function to be equivalent to the cost in the original state $\mathbf{x}$, a modified weight matrix may be considered such that $\boldsymbol{\varphi}^T\mathbf{Q}_\varphi\boldsymbol{\varphi} \approx \mathbf{x}^T\mathbf{Q}\mathbf{x}$. This can only be achieved exactly if the state itself is an eigenfunction of the Koopman operator; however, it can be sufficient requiring this only for a subset of states that enter the cost function. Alternatively, it is possible to estimate $\mathbf{x}$ via the inverse mapping φ^{-1}. Eigenfunctions may generally not be invertible exactly. Nevertheless, the inverse mapping may be approximated using multidimensional scaling as in [57] or learned jointly with φ itself using autoencoders [73]. More generally, the matrix $\mathbf{Q}_\varphi$ allows one to weight particular eigenfunction directions, which are related to properties of the underlying system and coherent structures. The selection of a specific set of eigenfunctions, in which a model is constructed and which are used to formulate the cost functional, is problem specific. However, given a target state $\mathbf{x}^{\mathrm{REF}}$ in the original state space, the associated target value of the eigenfunctions may be directly determined by evaluating the eigenfunctions on the target state, i.e. $\boldsymbol{\varphi}^{\mathrm{REF}} := \boldsymbol{\varphi}(\mathbf{x}^{\mathrm{REF}})$.

For the general case, it is possible to augment the state with the control input and include the derivative of the control as new input $\hat{\mathbf{u}} := \dot{\mathbf{u}}$:

$$\frac{\mathrm{d}}{\mathrm{d}t}\begin{bmatrix}\boldsymbol{\varphi}\\ \mathbf{u}\end{bmatrix} = \begin{bmatrix}\boldsymbol{\Lambda} & \mathbf{B}_\varphi\\ \mathbf{0} & \mathbf{0}\end{bmatrix}\begin{bmatrix}\boldsymbol{\varphi}\\ \mathbf{u}\end{bmatrix} + \begin{bmatrix}\mathbf{0}\\ \mathbf{I}_q\end{bmatrix}\hat{\mathbf{u}} \tag{29}$$

with $q\times q$ identity matrix $\mathbf{I}_q$. This may be interpreted as integral control. The cost functional is then given by

$$J = \frac{1}{2}\int_0^\infty \begin{bmatrix}\boldsymbol{\varphi}^T & \mathbf{u}^T\end{bmatrix}\begin{bmatrix}\mathbf{Q}_\varphi & \mathbf{0}\\ \mathbf{0} & \mathbf{R}\end{bmatrix}\begin{bmatrix}\boldsymbol{\varphi}\\ \mathbf{u}\end{bmatrix} + \hat{\mathbf{u}}^T\hat{\mathbf{R}}\hat{\mathbf{u}}\,\mathrm{d}t. \tag{30}$$

with some restrictions on $\hat{\mathbf{R}}$. Modifying the system structure, by moving the nonlinearity in the control term into the state dynamics, improves the tractability of the problem [11].

In the following, we will focus on multiple-input, control-affine systems (21), for which the dynamics in intrinsic coordinates becomes

$$\frac{\mathrm{d}}{\mathrm{d}t}\boldsymbol{\varphi}(\mathbf{x}) = \boldsymbol{\Lambda}\boldsymbol{\varphi}(\mathbf{x}) + \nabla_{\mathbf{x}}\boldsymbol{\varphi}(\mathbf{x})\cdot\mathbf{B}\mathbf{u} \tag{31}$$

with $\mathbf{\Lambda} = \mathrm{diag}(\lambda_1, \ldots, \lambda_r)$. Depending on the structure of $\boldsymbol{\varphi}(\mathbf{x})$ and $\mathbf{B}$, the actuation matrix $\mathbf{B}_\varphi = \nabla_\mathbf{x}\boldsymbol{\varphi}(\mathbf{x}) \cdot \mathbf{B}$ may be a function of $\mathbf{x}$. A state-dependent control term may be interpreted as a gain-scheduled control. A feedback controller is now sought in the Koopman representation of the form

$$\mathbf{u} = -\mathbf{c}_\varphi[\boldsymbol{\varphi}(\mathbf{x})] = -\mathbf{C}_\varphi(\mathbf{x})\boldsymbol{\varphi}(\mathbf{x}). \tag{32}$$

We may also consider reference tracking, $\mathbf{u} = -\mathbf{C}_\varphi(\mathbf{x})\left[\boldsymbol{\varphi}(\mathbf{x}) - \boldsymbol{\varphi}^{\mathrm{REF}}\right]$, with a modified cost functional (28). The objective is then to determine the gain function $\mathbf{C}_\varphi$ by minimizing $J(\boldsymbol{\varphi}, \mathbf{u})$ and the resulting control $\mathbf{u}$ may be directly applied to the original system (21), for which the control problem may be suboptimal. Generally, Koopman eigenfunction control can be used in two ways depending on which means of control one has access to: (a) internally driven swimmers or particles, which state is given by $\mathbf{x}$ and which dynamics are subject to an external field, such as a fluid flow or magnetic field; or (b) driving an external field, represented in terms of these eigenfunctions, in which these swimmers or particles drift.

4.4. Solving the optimal control problem

The model (31) may be combined with any model-based control strategy. In the following, we discuss ways to solve the optimal control problem formulated above using standard techniques.

In the simplest case, for which equation (31) becomes fully linear, the optimal gain matrix $\mathbf{C}_\varphi$ can be determined by solving the associated algebraic Riccati equation leading to a linear quadratic regulator (LQR) formulated in Koopman eigenfunctions. For the more general case, where the control term becomes nonlinear, other techniques are required. A common extension of LQR for nonlinear systems considers state-dependent state and control matrices as outlined in section A.3 and solves the state-dependent Riccati equation (A9). Here, the state dynamics would be constant and linear, i.e. $\mathbf{A} = \mathbf{\Lambda}$, and only the control matrix $\mathbf{B}_\varphi := \nabla_\mathbf{x}\varphi \cdot \mathbf{B}$ depends on the state $\mathbf{x}$:

$$\mathbf{Q} + \mathbf{P}\mathbf{\Lambda} + \mathbf{\Lambda}^T\mathbf{P} - \mathbf{P}\mathbf{B}_\varphi(\mathbf{x})\mathbf{R}^{-1}\mathbf{B}_\varphi^T(\mathbf{x})\mathbf{P} = \mathbf{0}. \tag{33}$$

We note that parametrizations for the dynamics (A8) in $\mathbf{x}$ are unique for scalar systems, but generally nonunique for multivariable systems [30]. In contrast, the state-dependent dynamics in eigenfunction coordinates (31) are unique with respect to $\mathbf{x}$ and $\mathbf{\Lambda}$ is constant. These are not a result from the factorization. The (non)uniqueness of the factorization is generally related to global optimal control and global optimal stability. However, further studies are required to connect these properties for solutions in eigenfunction coordinates to the state dynamics in $\mathbf{x}$.

We examine the effect of an error $\varepsilon\psi(\mathbf{x})$ in the representation of a Koopman eigenfunction, $\hat{\varphi}(\mathbf{x}) := \varphi(\mathbf{x}) + \varepsilon\psi(\mathbf{x})$, on its closed-loop dynamics based on (33) and provide an upper bound for the error (for details see appendix B). We assume control-affine dynamics (21) of the underlying system, access to full-state measurements $\mathbf{x}$, and control vector fields are known. Further, we reformulate $\mathbf{B}(\mathbf{x})\mathbf{u} := \sum_{i=1}^{q} \mathbf{b}_i(\mathbf{x})u_i$ for simplicity. The closed-loop dynamics of $\varphi(\mathbf{x})$ are then given by

$$\dot{\varphi}(\mathbf{x}) = -\sqrt{\lambda^2 + Q\mathbf{C}(\mathbf{x})\mathbf{R}^{-1}\mathbf{C}^T(\mathbf{x})}\varphi(\mathbf{x}) = -\sqrt{\mu}\varphi(\mathbf{x}), \tag{34}$$

where $\mu := \lambda^2 + Q\mathbf{C}(\mathbf{x})\mathbf{R}^{-1}\mathbf{C}^T(\mathbf{x})$. The upper bound for the error in μ due to the misrepresentation of $\varphi(\mathbf{x})$ due to $\varepsilon\psi(\mathbf{x})$ is

$$|\mu - \hat{\mu}| \leqslant \left| -\varepsilon\left(Q\mathbf{C}\mathbf{R}^{-1}\mathbf{D}^T + Q\mathbf{D}\mathbf{R}^{-1}\mathbf{C}^T + 2\lambda\frac{\nabla\psi\cdot\mathbf{f}}{\varphi(\mathbf{x})}\right) - \varepsilon^2\left(Q\mathbf{D}\mathbf{R}^{-1}\mathbf{D}^T + \frac{(\nabla\psi\cdot\mathbf{f})^2}{\varphi^2(\mathbf{x})}\right)\right|. \tag{35}$$

where $\mathbf{C}(\mathbf{x}) := \nabla\varphi(\mathbf{x}) \cdot \mathbf{B}(\mathbf{x})$ and $\mathbf{D}(\mathbf{x}) := \nabla\psi(\mathbf{x}) \cdot \mathbf{B}(\mathbf{x})$ are the control terms associated with $\varphi(\mathbf{x})$ and $\psi(\mathbf{x})$, respectively. For small $\varphi(\mathbf{x})$ the contribution of $\varepsilon\psi(\mathbf{x})$ becomes important/may be dominant.

More generally, Koopman control in eigenfunction coordinates may be combined with any model-based control approach. Under certain conditions, it may also be possible to feedback linearize the dynamics [58]. The data-driven identification of Koopman eigenfunctions can be challenging and they may only be approximated accurately in a certain domain. Further, dynamics may also drift away from the situations captured in the training data due to external disturbances. Especially in these cases it is advantageous to couple the resulting model with a receding horizon estimator and controller to adapt quickly to changing conditions. In particular, model predictive control has gained increasing popularity over the last decade due to its success in a wide range of applications and its ability to incorporate customized cost functions and constraints [3, 26, 39].

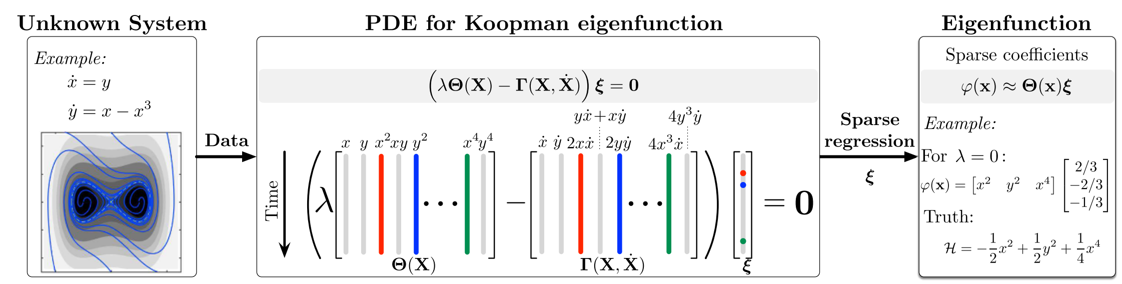

Figure 5. Identification of Koopman eigenfunctions from data using implicit-SINDy.

5. Identifying Koopman eigenfunctions from data

The overarching goal of this work is to control nonlinear systems in intrinsic Koopman eigenfunction coordinates. A leading method for approximating the Koopman operator is EDMD relying on a set of basis or dictionary functions. Here, we aim to address the well-known closure issue, i.e. the model may not be closed in the set of basis functions and can therefore have spurious eigenfunctions, by assuming an eigenfunction perspective. Approximating these eigenfunctions from data is an ongoing challenge. Building on EDMD, we propose a strategy to directly identify dominant Koopman eigenfunctions associated with lightly damped eigenvalues, that can then be utilized to construct low-dimensional, closed models. Further, we show that it is possible to sparsify the state-transition matrix $\mathbf{K}$ of EDMD to improve the representation of eigenfunctions within the selected basis.

It has long been recognized that numerical regularization via the truncation of the SVD in the computation of the pseudoinverse, as it is done for DMD/EDMD, is crucial to reduce noise corruption. However, this does not produce a sparser approximation of $\mathbf{K}$, which is crucial for systems that are inherently sparse in their representation. An additional $L1$ regularization is here advantageous as it is able to improve the predictive power of the model and eigenfunctions become more accurately represented in the chosen function library preventing overfitting. Interestingly, the infinitesimal generator of the Koopman operator may be sparse even when the Koopman operator itself is not [60]. However, even in these cases, the approach may benefit from a sparsity constraint to counteract spurious non-zero entries arising from noise and numerical approximation. More generally, non-compactness or continuous spectra of the Koopman operator can pose issues for the numerical analysis requiring some form of regularization (see [42] for a detailed discussion for the Koopman operator and [41] regarding the Perron-Frobenius operator).

In the following we formulate a framework using sparsity-promoting techniques to identify Koopman eigenfunctions directly building on the partial differential equation (PDE) governing the evolution of an eigenfunction. Applying the chain rule to (12) yields

$$\frac{\mathrm{d}}{\mathrm{d}t}\varphi(\mathbf{x}) = \nabla\varphi(\mathbf{x})\cdot\dot{\mathbf{x}} = \nabla\varphi(\mathbf{x})\cdot\mathbf{f}(\mathbf{x}). \tag{36}$$

Combined with (12), this results in a linear PDE for the eigenfunction $\varphi(\mathbf{x})$:

$$\nabla\varphi(\mathbf{x})\cdot\mathbf{f}(\mathbf{x}) = \lambda\varphi(\mathbf{x}). \tag{37}$$

This formulation assumes continuous and differentiable dynamics and that the eigenfunctions are smooth [83].

Spectral properties of the Koopman operator have been shown to relate to intrinsic time scales, geometrical properties, and the long-term behavior of dynamical systems [68, 76, 79, 84]. It has been shown [82], that the evolution of observables can be described by a linear expansion in Koopman eigenfunctions for systems which consist only of the point spectrum, i.e. smooth dynamical systems exhibiting, e.g. hyperbolic fixed points, limit cycles and tori. If systems with a mixed spectrum are considered, it may be possible to restrict the following analysis to the point spectrum as in [32].

5.1. Data-driven discovery of continuous-time eigenfunctions

Sparse identification of nonlinear dynamics (SINDy) [22] is used to identify Koopman eigenfunctions for a particular value of λ. This formalism assumes that the system has a point or mixed spectrum, for which eigenfunctions with distinct eigenvalues exist. A schematic is displayed in figure 5.

Algorithm 1. Direct discovery of eigenfunctions based on the implicit formulation (42).

Initialize: $\boldsymbol{\Lambda}^{guess} = \mathrm{eigs}(\boldsymbol{\Theta}(\mathbf{X})^{\dagger}\boldsymbol{\Gamma}(\mathbf{X},\dot{\mathbf{X}}))\}$
for each eigenvalue λ_i in $\boldsymbol{\Lambda}^{guess}$ **do**
  Initialize: $\lambda = \lambda_i^{guess}$
  while λ not converged **do**
    $\mathbf{M} := \boldsymbol{\Gamma}(\mathbf{X},\dot{\mathbf{X}}) - \lambda\boldsymbol{\Theta}(\mathbf{X})$
    $\mathbf{N} := \mathrm{null}(\mathbf{M})$
    for each row l in $\mathbf{N}$ **do**
      $\mathbf{q}_0 := (\mathbf{N}(l,:)/\mathrm{norm}(\mathbf{N}(l,:)))^T$
      $q_{mtx}(:,l) := \mathrm{adm}(\mathbf{N},\mathbf{q}_0,\ \alpha,\ \mathit{MaxIter},\ \mathit{tolerance});$
      $\boldsymbol{\Xi}(:,l) = \mathbf{N}\mathbf{q}_{mtx}(:,l)$
    end for
    for each column l in $\boldsymbol{\Xi}$ **do**
      $\boldsymbol{\Xi}(:,l) := \mathrm{soft\_thresholding}(\boldsymbol{\Xi}(:,l),\alpha)$
      $\boldsymbol{\Xi}(:,l) := \mathrm{normalize}(\boldsymbol{\Xi}(:,l))$
      $\mathit{Error}(l) := \mathrm{norm}(\boldsymbol{\Theta}(\mathbf{X}^{test})\boldsymbol{\Xi}(:,l) - \mathrm{e}^{\lambda \mathbf{t}^{test}}\boldsymbol{\Theta}(\mathbf{x}_0^{test})\boldsymbol{\Xi}(:,l))$
    end for
    $\mathit{best} := \min(\mathit{Error})$
    $\boldsymbol{\xi} := \boldsymbol{\Xi}(:,\mathit{best})$
    Update $\lambda := (\boldsymbol{\xi}^T\boldsymbol{\Theta}(\mathbf{X})^{\dagger}\boldsymbol{\Gamma}(\mathbf{X},\dot{\mathbf{X}})\boldsymbol{\xi})/(\boldsymbol{\xi}^T\boldsymbol{\xi})$
  end while
  $\mathbf{T}(:,i) = \boldsymbol{\xi}$
  $\boldsymbol{\Lambda}(i,i) = \lambda$
end for
return $\boldsymbol{\Lambda}$, $\mathbf{T}$

First, we build a library of candidate functions:

$$\boldsymbol{\Theta}(\mathbf{x}) = \begin{bmatrix}\theta_1(\mathbf{x}) & \theta_2(\mathbf{x}) & \cdots & \theta_p(\mathbf{x})\end{bmatrix}. \tag{38}$$

We choose $\boldsymbol{\Theta}$ large enough so that the Koopman eigenfunction may be well approximated in this library:

$$\varphi(\mathbf{x}) \approx \sum_{k=1}^{p}\theta_k(\mathbf{x})\xi_k = \boldsymbol{\Theta}(\mathbf{x})\boldsymbol{\xi}. \tag{39}$$

Given data $\mathbf{X} = [\mathbf{x}_1\,\mathbf{x}_2\cdots\mathbf{x}_m]$, the time derivative $\dot{\mathbf{X}} = [\dot{\mathbf{x}}_1\,\dot{\mathbf{x}}_2\cdots\dot{\mathbf{x}}_m]$ can be approximated numerically from $\mathbf{x}(t)$ if not measured directly [22]. The total variation derivative [28] is recommended for noise-corrupted measurements. It is then possible to build a data matrix $\boldsymbol{\Theta}(\mathbf{X})$:

$$\boldsymbol{\Theta}(\mathbf{X}) = \begin{bmatrix}\theta_1(\mathbf{X}^T) & \theta_2(\mathbf{X}^T) & \cdots & \theta_p(\mathbf{X}^T)\end{bmatrix}. \tag{40}$$

Moreover, we can define a library of directional derivatives, representing the possible terms in $\nabla\varphi(\mathbf{x})\cdot\mathbf{f}(\mathbf{x})$ from (37): $\boldsymbol{\Gamma}(\mathbf{x},\dot{\mathbf{x}}) = [\nabla\theta_1(\mathbf{x})\cdot\dot{\mathbf{x}}\,\nabla\theta_2(\mathbf{x})\cdot\dot{\mathbf{x}}\cdots\nabla\theta_p(\mathbf{x})\cdot\dot{\mathbf{x}}]$. It is then possible to construct $\boldsymbol{\Gamma}$ from data:

$$\boldsymbol{\Gamma}(\mathbf{X},\dot{\mathbf{X}}) = \begin{bmatrix}\nabla\theta_1(\mathbf{X}^T)\cdot\dot{\mathbf{X}} & \nabla\theta_2(\mathbf{X}^T)\cdot\dot{\mathbf{X}} & \cdots & \nabla\theta_p(\mathbf{X}^T)\cdot\dot{\mathbf{X}}\end{bmatrix}. \tag{41}$$

For a specific eigenvalue λ, the Koopman PDE in (37) may be evaluated on data, yielding

$$\left(\lambda\boldsymbol{\Theta}(\mathbf{X}) - \boldsymbol{\Gamma}(\mathbf{X},\dot{\mathbf{X}})\right)\boldsymbol{\xi} = 0. \tag{42}$$

The formulation in (42) is implicit, so that $\boldsymbol{\xi}$ will be in the null-space of the matrix $\lambda\boldsymbol{\Theta}(\mathbf{X}) - \boldsymbol{\Gamma}(\mathbf{X},\dot{\mathbf{X}})$. The right null-space of (42) for a given λ is spanned by the right singular vectors of $\lambda\boldsymbol{\Theta}(\mathbf{X}) - \boldsymbol{\Gamma}(\mathbf{X},\dot{\mathbf{X}}) = \mathbf{U}\boldsymbol{\Sigma}\mathbf{V}^*$ (i.e. columns of $\mathbf{V}$) corresponding to zero-valued singular values. It is possible to identify the few active terms in an eigenfunction by finding the sparsest vector in the null-space [95], which is used, e.g. in the implicit-SINDy algorithm [74]. This is a nonconvex approach based on alternating directions (adm) with linear scaling [95], which can be adapted to our problem. In this formulation, the eigenvalues λ are not known *a priori*, and must be learned online along with the approximate eigenfunction. In algorithm 1, we propose an implicit formulation, which starts with an initial guess of the eigenvalues given by the least-squares solution, and subsequently alternates between an searching for the sparsest vector in the null-space [95] and updating of the eigenvalue. As the approach in [95] depends on the initial condition, we evaluate all initial conditions given by each row in the nullspace $\mathbf{N} := \text{null}(\boldsymbol{\Gamma}(\mathbf{X}, \dot{\mathbf{X}}) - \lambda\boldsymbol{\Theta}(\mathbf{X}))$. An additional soft-thresholding with parameter α and validation on a test dataset is applied to select the best eigenvector for each initial condition. While the approach has been observed to converge to accurate eigenvalues in clean data, the found eigenvector in the solution set may not be unique. This approach solves for each eigenpair separately; however, it may also be possible to extend it to solve for eigenpairs jointly which is part of ongoing research. From a practical standpoint, data in $\mathbf{X}$ does not need to be sampled from full trajectories, but can be obtained using more sophisticated strategies such as latin hypercube sampling or sampling from a distribution over the phase space. It may also be possible to directly identify a recursion relationship to obtain a power series expansion as shown in appendix C and in [77].

Koopman eigenfuntions and eigenvalues can also be determined as the solution to the eigenvalue problem $\boldsymbol{\xi}_\alpha \mathbf{K} = \lambda_\alpha \boldsymbol{\xi}_\alpha$, where $\mathbf{K} = \boldsymbol{\Theta}^\dagger \boldsymbol{\Gamma}$ is obtained via least-squares (LS) regression. While many eigenfunctions are spurious, i.e. these eigenfunctions do not behave linearly as predicted by the corresponding eigenvalue, those corresponding to lightly damped eigenvalues can be well approximated [20, 68], and a reduced-order Koopman model may developed on these coordinates (see also section 2). The accuracy of eigenfunctions of $\mathbf{K}$ can be improved, by improving the recovery of $\mathbf{K}$ itself, which can be achieved by sparsifying $\mathbf{K}$ directly. The minimization problem

$$\min_{\mathbf{k}_i} ||\nabla\theta_i(\mathbf{X}^T) \cdot \dot{\mathbf{X}} - \boldsymbol{\Theta}(\mathbf{X})\mathbf{k}_i^T||_2^2 + \rho(\mathbf{k}_i), \quad \forall \mathbf{k}_i, i = 1, \ldots, p, \tag{43}$$

where ρ is a regularization term that promotes the sparsity of $\mathbf{k}_i$, i.e. the number of non-zero coefficients, is solved separately for each row in $\mathbf{K} = [\mathbf{k}_1^T, \ldots, \mathbf{k}_p^T]$. For instance, an L_1 constraint on the coefficients in $\mathbf{k}_i$ may be chosen and $\mathbf{k}_i$ may equivalently be determined as in SINDy [22]. In general, the problem (43) can be solved using standard techniques, such as LASSO [98, 112], least angle regression [38], or an iterated least-squares thresholding method [22].

This formulation is closely related to the gEDMD framework [60], a generalization of the EDMD method to approximate the infinitesimal generator of the Koopman operator. The gEDMD least-squares formulation is solved here row-wise with an additional sparsity constraint. There are also similarities to sparsity-promoting DMD [55] and variants [52, 54], which aims to reconstruct a signal through a sparse combination of modes/eigenfunctions, which have been computed from a least-squares solution. In contrast to these works, we argue that the sparse representation of eigenfunctions themselves should be promoted. Alternatively, it is also possible to use the dominant terms in accurately identified eigenfunctions, generally associated with lightly damped eigenvalues, as guidance to select observables to regress on. Since the first appearance of this article, further promising methods have been proposed to identify Koopman eigenfunctions directly [48, 65, 88].

5.2. Data-driven discovery of discrete-time eigenfunctions

In discrete-time, an eigenfunction evaluated at a number of data points in $\mathbf{X}$ will satisfy

$$\begin{bmatrix}\lambda\varphi(\mathbf{x}_1) & \ldots & \lambda\varphi(\mathbf{x}_m)\end{bmatrix}^T = \begin{bmatrix}\varphi(\mathbf{x}_2) & \ldots & \varphi(\mathbf{x}_{m+1})\end{bmatrix}^T. \tag{44}$$

Again, searching for such an eigenfunction $\varphi(\mathbf{x})$ in a library $\boldsymbol{\Theta}(\mathbf{x})$ yields the matrix system:

$$(\lambda\boldsymbol{\Theta}(\mathbf{X}) - \boldsymbol{\Theta}(\mathbf{X}'))\,\boldsymbol{\xi} = 0, \tag{45}$$

where $\mathbf{X}' = \begin{bmatrix}\mathbf{x}_2 & \mathbf{x}_3 & \cdots & \mathbf{x}_{m+1}\end{bmatrix}$ is a time-shifted matrix. This formalism directly identifies the functional representation of a Koopman eigenfunction with eigenvalue λ.

If we seek the best *least-squares* fit to (45), this reduces to the extended DMD [117] formulation:

$$\lambda\boldsymbol{\xi} = \boldsymbol{\Theta}^\dagger\boldsymbol{\Theta}'\boldsymbol{\xi}. \tag{46}$$

Again, it is necessary to confirm that predicted eigenfunctions actually behave linearly on trajectories.

5.3. Koopman model reduction and validation

For any data-driven modeling framework cross-validation is critical to ensure predictive and generalization capabilities. Approximations of the Koopman operator allow a systematic evaluation based on its linearity property. We can learn a finite-rank approximation using any EDMD-like method or learn eigenfunctions directly. In either case, it is critical to validate that any candidate eigenfunction $\varphi(\mathbf{x}(t))$ actually behaves linearly on trajectories $\mathbf{x}(t)$ as the eigenvalue λ predicts. The error of an eigenfunction can be defined as

$$E = ||\varphi(\mathbf{x}(t)) - \mathrm{e}^{\lambda t}\varphi(\mathbf{x}(0))||^2 \tag{47}$$

evaluated on a test trajectory $\mathbf{x}(t)$ and identified eigenfunctions can be ranked according to the error E. All eigenfunctions with error below a threshold may then be used to construct a reduced-order model:

$$\varphi(\mathbf{x}) = \boldsymbol{\Lambda}\varphi + \nabla\varphi(\mathbf{x}) \cdot \mathbf{B}\mathbf{u} \tag{48}$$

analogous to equation (31). This model is closed and behaves linearly by design and we demonstrate in the following its increased predictive power.

6. Example: system with a slow manifold

6.1. Identification of eigenfunctions and models

We consider a system with quadratic nonlinearity that gives rise to a slow manifold [114]:

$$\frac{\mathrm{d}}{\mathrm{d}t}\begin{bmatrix} x_1 \\ x_2 \end{bmatrix} = \begin{bmatrix} \mu x_1 \\ \lambda(x_2 - x_1^2) \end{bmatrix} \tag{49}$$

with $\mu = -0.1$ and $\lambda = -1$. In the following, we apply the methods outlined in section 5 to the dynamical system (49). For all models, a library of the first nine monomials (up to the third degree) is considered. Noise corruption in measurement data can be particularly problematic. Here, we examine the recovery of eigenfunctions and prediction performance for different noise magnitudes $\eta = 0.1$ and $\eta = 0.9$. Further, reduced-order models are constructed based on eigenpairs $(\beta, \varphi(\mathbf{x}))$ that are deemed accurate, i.e. have a small L_2 error when compared with the prediction using the associated eigenvalue, here denoted by β. The threshold for the selection of eigenfunctions is 1 and 3 for noise magnitudes $\eta = 0.1$ and $\eta = 0.9$, respectively. The L_1 regularized problem is solved using the iterative least-squares thresholding algorithm (ITLS) as in SINDy [22] and least angle regression (LARS) [38]; however, detailed results are only shown for LARS as these have equivalent performance. LARS has the advantage that the number of iterations scales with the number of candidate functions; only ten iterations are required here. The sparse solution is then selected when there is minimal improvement in the absolute value of correlation with the evolving residual. The soft thresholding parameter in the implicit formulation is set to $\alpha = 0.1$ and $\alpha = 0.2$ for $\eta = 0.1$ and $\eta = 0.9$, respectively.

The results are displayed in figures 6 and 7 for the two noise cases. We observe that with increasing noise level, the EDMD state transition matrix becomes denser due to overfitting (see (d)). In contrast, the implicit approach and L_1-regularized EDMD (termed 'LARS' or 'ITLS' in the following) yield sparse matrices, which is more apparent for large noise magnitude. Note that the state matrix for the implicit formulation is reconstructed using the identified eigenfunctions on the set of candidate functions for visualization purposes, i.e. there are many zero entries and candidate functions that do not contribute to the actual dynamics. Lightly damped eigenfunctions can be recovered for all approaches. Eigenfunctions, or specifically eigenpairs $(\beta, \varphi(\mathbf{x}))$, are deemed as recovered, if the prediction error falls below a threshold (marked as dashed line in (f)). The prediction error is computed by evaluating the eigenfunction on a test trajectory and comparing it with the evolution as predicted by the associated eigenvalue; the evolution is displayed in (e). These *good* eigenpairs (colored as blue bars in (f)) are then used to construct reduced-order models (ROMs), that are by design linear and closed (subject to small errors). Note that solution from the implicit formulation may not be unique, i.e. there are several identical eigenpairs. However, only unique eigenpairs are used to construct the reduce-order model. This is the reason why, e.g. in figure 6(f), the error for all eigenpairs falls below the threshold, but only unique ones (marked in blue) are selected to construct the ROM.

For small noise magnitude (figure 6), the identified models and ROMs perform all well, except the EDMD-based ROM, as one crucial eigenfunction associated with $\beta = -0.19$ falls above the threshold and is not selected. The eigenvalue is correct, but not the associated eigenfunction. If the eigenfunction is included in the model (yellow bar in (f) and yellow dashed line in (g)), i.e. the model is constructed from blue and yellow marked eigenpairs, it yields a similar performance as the full-state EDMD model. It can also be observed that even in the low noise setting sparsification yields improvements. We note that the full-state model and ROM obtained from the implicit formulation are identical, as all discovered eigenpairs fall below the threshold (in (f)) and only unique pairs are selected to construct either model. We note that the 4D-ROM from the implicit formulation can achieve better accuracy with one dimension lower compared with EDMD and the sparse EDMD model identified using LARS. Moreover, while all eigenpairs from the implicit formulation are accurate, both EDMD and LARS yield also non-physical eigenfunctions. The overall L_2 prediction error on the test trajectory in the original state is summarized for the full-state models and ROMs in (b) and (c), respectively.

For higher noise levels (figure 7), the performance differences become more apparent. LARS still yields several more accurate eigenfunctions than EDMD, so that LARS and the LARS-ROM significantly

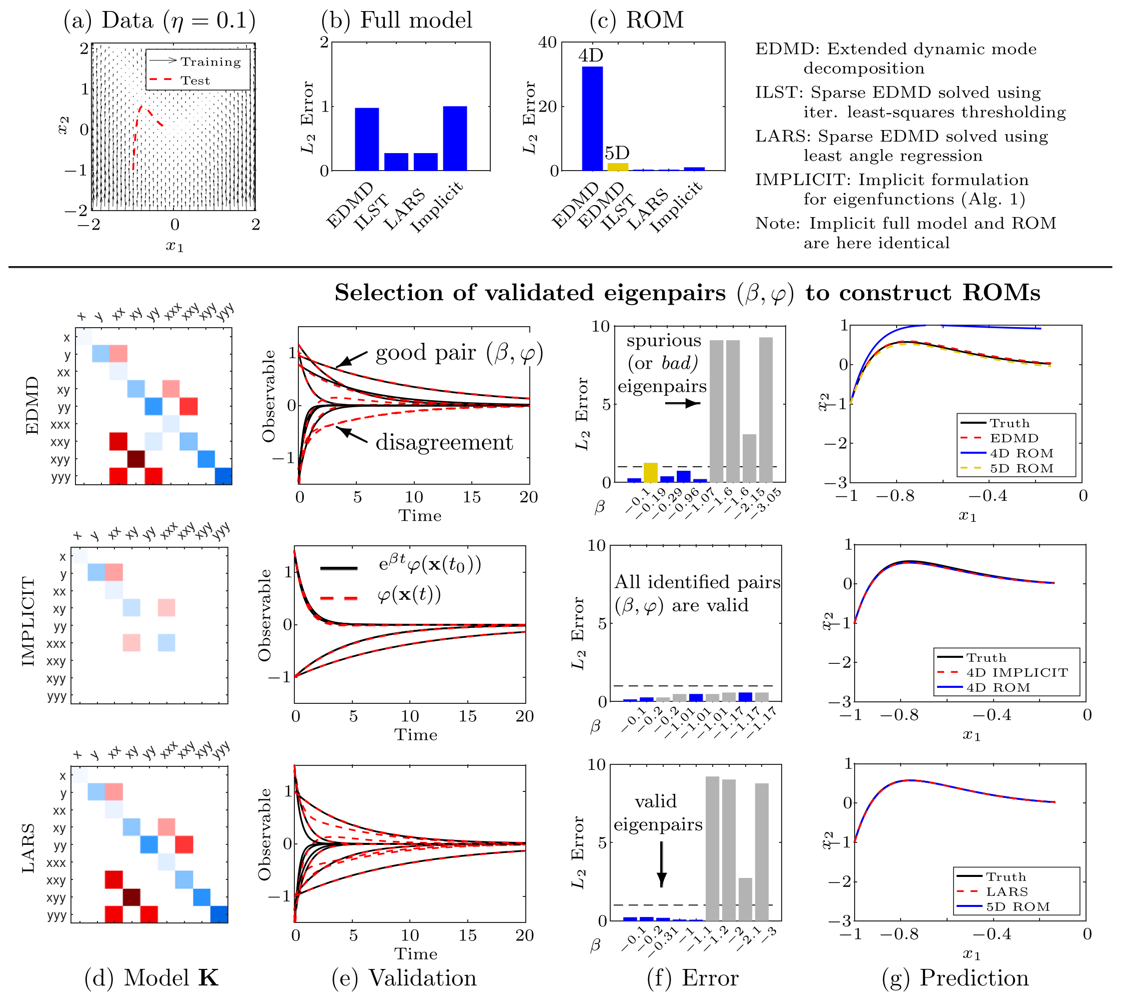

Figure 6. Model comparison for the slow manifold system with noise level $\eta = 0.1$: (a) training and test data, (b) state prediction error on test data for each identified model, (c) state prediction error on test data for each identified reduced-order model (ROM), (d) transition matrix on set of measurement functions, (e) eigenpairs $(\beta, \varphi(\mathbf{x}))$ validated on test trajectory (marked blue if below threshold (dashed line)), (f) prediction error for each eigenpair $(\beta, \varphi(\mathbf{x}))$ (error between trajectory as predicted by eigenvalue and by evaluating eigenfunction on test trajectory), (g) state prediction using model $\mathbf{K}$ and ROM constructed from validated (or *good*) eigenfunctions (marked in blue/yellow in (f)). For details see text.

outperform EDMD and the EDMD-based ROM. The performance of EDMD does not improve here by truncating the SVD when computing the pseudo-inverse. The implicit formulation is more noise sensitive, as it is searching for eigenfunctions in the nullspace of a matrix (42), and is only able to discover one accurate eigenfunction. Interestingly, despite this caveat, the 2D model is able to outperform EDMD and the EDMD-based ROM. The implicit model is unable to predict the exact transient behavior; however, it accurately predicts the convergence to the steady state. The implicit ROM model, however, is insufficient with just one eigenfunction $\varphi(\mathbf{x}) = x_1$ and is unable to predict the evolution of the second state x_2. When selecting one or two additional eigenfunctions for the EDMD-based ROM (in yellow shown in (g) for two additional eigenfunctions, i.e. in total six eigenfunctions marked by blue and yellow in (f)), the prediction performance improves considerably, although it is still unable to predict the steady-state behavior.

Summarizing, EDMD is suffering from overfitting and sparsity-promoting formulations can yield significant performance enhancements. Model validation in terms of eigenfunctions is a crucial step and can be used to construct better performing and lower-dimensional reduced-order models. More generally, these results also demonstrate the importance of not just selecting *good*, but also the *right* eigenfunctions.

6.2. Control design

We now demonstrate control in intrinsic Koopman coordinates for the controlled system:

$$\frac{\mathrm{d}}{\mathrm{d}t}\begin{bmatrix} x_1 \\ x_2 \end{bmatrix} = \begin{bmatrix} \mu x_1 \\ \lambda(x_2 - x_1^2) \end{bmatrix} + \mathbf{B}\,u \tag{50}$$

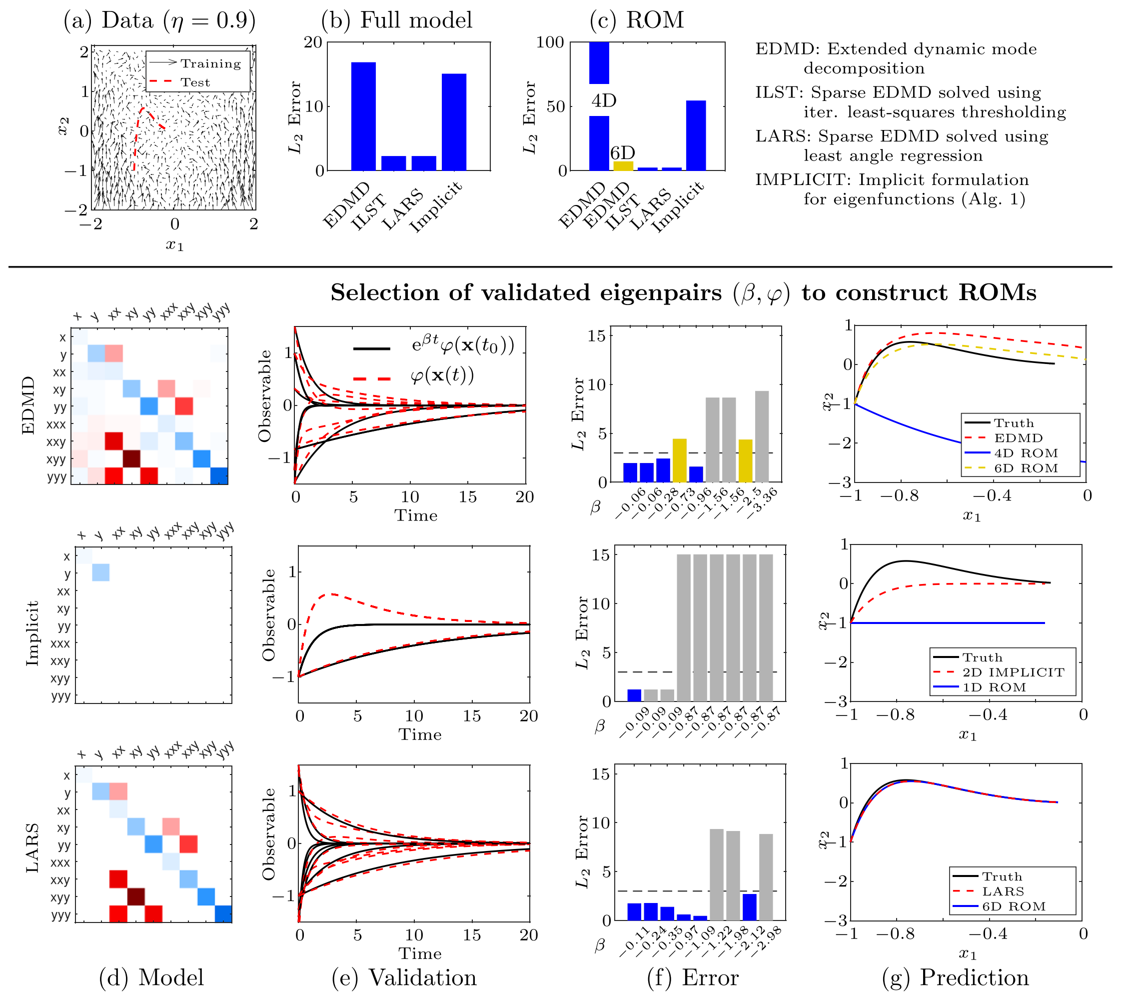

Figure 7. Model comparison for the slow manifold system as in figure 6 but with higher measurement noise level $\eta = 0.9$. The ROM model error displayed in (c) is cut at 100. For details see figure 6.

where the control vector is $\mathbf{B} \in \mathbb{R}^2$. This system can be represented as a finite-dimensional, linear system in a special choice of observable functions, making it amenable to optimal control [20]. KRONIC in intrinsic coordinates provides a powerful alternative if the system does not allow for a fully controllable, linear representation.

The system exhibits slow and fast dynamics for $|\lambda| \ll |\mu|$ and has a single fixed point at the origin. This nonlinear system can be embedded in a higher-dimensional space $(y_1, y_2, y_3) = (x_1, x_2, x_1^2)$ where the unforced dynamics form a closed linear system in a Koopman-invariant subspace:

$$\frac{\mathrm{d}}{\mathrm{d}t}\begin{bmatrix} y_1 \\ y_2 \\ y_3 \end{bmatrix} = \underbrace{\begin{bmatrix} \mu & 0 & 0 \\ 0 & \lambda & -\lambda \\ 0 & 0 & 2\mu \end{bmatrix}}_{\mathbf{K}} \begin{bmatrix} y_1 \\ y_2 \\ y_3 \end{bmatrix} + \underbrace{\begin{bmatrix} 1 & 0 \\ 0 & 1 \\ 2y_1 & 0 \end{bmatrix}}_{=\mathbf{B}_y} \mathbf{B}\, u. \tag{51}$$

However, $\mathbf{B}_y$ may be a function of $\mathbf{y}$, and hence of state $\mathbf{x}$, depending on the specific choice of $\mathbf{B}$. Koopman eigenfunctions of the unforced system, i.e. $\mathbf{B} \equiv [0\ 0]^T$, are $\varphi_\mu = x_1$ and $\varphi_\lambda = x_2 - bx_1^2$ with $b = \frac{\lambda}{\lambda - 2\mu}$ with eigenvalues λ and μ, respectively. These eigenfunctions remain invariant under the Koopman operator $\mathbf{K}$ and can be interpreted as intrinsic coordinates. Note that $\varphi_{p\beta} := \varphi_\beta^p$ are also Koopman eigenfunctions with eigenvalue $p\beta$ for $p \in \mathbb{N}$ (and $p \in \mathbb{Z}$ for non-vanishing $\varphi_{p\beta}$).

The dynamics of the Koopman eigenfunctions are affected by the additional control term $\mathbf{B} \neq [0\ 0]^T$ according to (see also equation (31))

$$\frac{\mathrm{d}}{\mathrm{d}t}\boldsymbol{\varphi} = \begin{bmatrix} \mu & 0 & 0 \\ 0 & \lambda & 0 \\ 0 & 0 & 2\mu \end{bmatrix} \boldsymbol{\varphi} + \begin{bmatrix} 1 & 0 \\ -2bx_1 & 1 \\ 2x_1 & 0 \end{bmatrix} \cdot \mathbf{B}\, u. \tag{52}$$

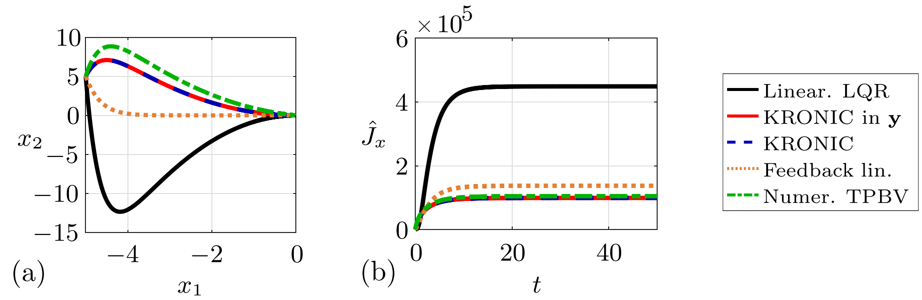

Figure 8. LQR for $\mathbf{B} = [0\ \ 1]^T$, $\mu = -0.1$ and $\lambda = 1$ using standard linearization, truncated Koopman in $\mathbf{y}$ and $\boldsymbol{\varphi}$ (KRONIC) compared with the solution of the nonlinear control problem (TPBV) and feedback linearization: (a) phase plot and (b) cost evolution. KRONIC is outperforming all other approaches.

Here, the first term represents the unforced, uncoupled, linear dynamics of the eigenfunctions and the second term a possibly state-dependent control term $\nabla\varphi \cdot \mathbf{B}$, that incorporates the effect of control on each eigenfunction.

The controller shall stabilize the unstable fixed point at the origin if either μ or λ are unstable. The control objective is to minimize the quadratic cost function

$$J_x = \int_0^\infty \mathbf{x}^T\mathbf{Q}\mathbf{x} + R\,u^2\,\mathrm{d}t \tag{53}$$

with $\mathbf{Q} = \left[\begin{smallmatrix}1 & 0\\ 0 & 1\end{smallmatrix}\right]$ and $R = 1$, weighing state and control expenditures equally. Analogously, we can define a cost function in observable functions,

$$J_y = \int_0^\infty \mathbf{y}^T\mathbf{Q}_y\mathbf{y} + R\,u^2\,\mathrm{d}t, \quad \mathbf{Q}_y = \begin{bmatrix} \mathbf{Q} & \begin{matrix}0\\0\end{matrix} \\ \begin{matrix}0 & 0\end{matrix} & 0 \end{bmatrix}, \tag{54}$$

and in intrinsic coordinates,

$$J_\varphi = \int_0^\infty \boldsymbol{\varphi}^T\mathbf{Q}_\varphi\boldsymbol{\varphi} + R\,u^2\,\mathrm{d}t, \quad \mathbf{Q}_\varphi = \begin{bmatrix} \mathbf{Q} & \begin{matrix}0\\b\end{matrix} \\ \begin{matrix}0 & b\end{matrix} & b^2 \end{bmatrix}. \tag{55}$$

Here, $\mathbf{Q}_y$ and $\mathbf{Q}_\varphi$ are chosen to yield the same cost in $\mathbf{x}$. Linear optimal control is then directly applied to (52) to derive the control law, which is then incorporated in (50). The controller is linear in $\mathbf{y}$ and $\boldsymbol{\varphi}$ and yields a nonlinear controller in the state $\mathbf{x}$:

$$\begin{aligned} u_y &= -\mathbf{C}_y\mathbf{y} = -\begin{bmatrix} C_{y,1} & C_{y,2}\end{bmatrix}\begin{bmatrix}x_1\\x_2\end{bmatrix} - C_{y,3}x_1^2 \\ u_\varphi &= -\mathbf{C}_\varphi\boldsymbol{\varphi} = -\begin{bmatrix} C_{\varphi,1} & C_{\varphi,2}\end{bmatrix}\begin{bmatrix}x_1\\x_2\end{bmatrix} - (C_{\varphi,3} - bC_{\varphi,1})x_1^2, \end{aligned}$$

where $\mathbf{C}_y \in \mathbb{R}^{1\times 3}$ and $\mathbf{C}_\varphi \in \mathbb{R}^{1\times 3}$ are the control gain vectors in observable or intrinsic coordinates, respectively.

6.3. Stabilization with unstable fast dynamics

First, we consider the system with $\mu = -0.1$ and $\lambda = 1$ with an unstable x_2 direction. The control vector is $\mathbf{B} = [0\ 1]^T$, resulting in a constant vector in $\mathbf{y}$ or $\boldsymbol{\varphi}$ coordinates, $\mathbf{B}_y = \mathbf{B}_\varphi = [0\ 1\ 0]^T$. Note that the first direction is uncontrollable, but also stable.

Standard LQR results are compared (see figure 8) for the linearized dynamics, truncated Koopman system in $\mathbf{y}$, truncated Koopman system in $\boldsymbol{\varphi}$ (KRONIC), as well as with feedback linearization [58] ($u_{\mathrm{FL}} = \lambda x_1^2 - \mathbf{C}_{\mathrm{FL}}\mathbf{x}$) and with numerically solving the nonlinear control problem as a two-point boundary value problem (TPBV), with performance evaluated in terms of the cumulative cost $\hat{J}_x^t = \sum_{\tau=0}^t J_x(\tau)$. Both controllers, in observable functions and intrinsic coordinates, achieve the same performance and outperform linearized LQR and feedback linearization. The results for the truncated Koopman system in observables correspond to those presented in [20]. There is no difference between those results and the control results of the system in intrinsic coordinates, as these systems are connected via an invertible linear transformation. One advantage of a formulation in intrinsic coordinates will become apparent in the next case, where the stable and unstable directions are reversed.

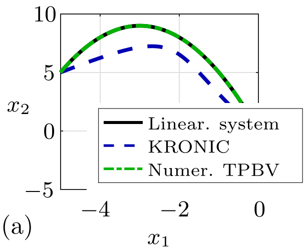

(a)

(b)

$\times 10^4$	KRONIC	Num. TPBV	Linear. LQR
$\hat{J}^T_{\mathbf{x}}$	1.660	1.337	1.337
$\hat{J}^T_{\boldsymbol{\varphi}}$	1.232	1.335	1.335

Figure 9. Control for $\mathbf{B} = [1\ 0]^T$, $\mu = 0.1$ and $\lambda = -1$ comparing KRONIC (56) by solving the SDRE, Num. TPBV, and LQR on the linearized dynamics: (a) phase plot, and (b) cumulative control performance over $T = 50$ time units. Note that the cost for KRONIC can not be directly compared with TPBV and linear. LQR, as the controller in the latter two is optimized with respect to J_x, while the former is optimized for $J_{\boldsymbol{\varphi}}$.

6.4. Stabilization with unstable slow dynamics

We now consider (50) where the stable and unstable directions are reversed, i.e. $\mu = 0.1$ and $\lambda = -1$. The control input now affects the first state x_1 with $\mathbf{B} = [1\ 0]^T$, otherwise this state is uncontrollable. As elaborated in [20], in this case the linear system in observables (51) will become nonlinear in the control term and, more importantly, will become unstabilizeable as the third state y_3 has a positive eigenvalue 2μ. Analogously, the Koopman system in intrinsic coordinates has an uncontrollable, unstable direction in $\varphi_{2\mu}$. However, the dynamics of the Koopman eigenfunctions are uncoupled, thus the third direction can be discarded and the controller is developed in the controllable subspace:

$$\frac{\mathrm{d}}{\mathrm{d}t}\begin{bmatrix}\varphi_\mu \\ \varphi_\lambda\end{bmatrix} = \begin{bmatrix}\mu & 0 \\ 0 & \lambda\end{bmatrix}\begin{bmatrix}\varphi_\mu \\ \varphi_\lambda\end{bmatrix} + \begin{bmatrix}1 \\ -2bx_1\end{bmatrix} u. \tag{56}$$

Note that the third direction $\phi_{2\mu}(x)$ is a harmonic of $\phi_\mu(x)$, i.e. $\phi_{2\mu} = \phi_\mu^2$. Thus, these two directions may not be independently controllable with a single input. Here, the controller for $\mathbf{x}$ is determined by solving the SDRE (see section 4.3) at each time instant to account for the nonlinear control term. In a truncated Koopman eigenfunction system like in this example, the weights in $J_{\boldsymbol{\varphi}}$ can generally not be modified to directly replicate the cost $J_{\mathbf{x}}$. Here, the weights for $J_{\mathbf{x}}$ are $\mathbf{Q} = \texttt{eye}(2)$ and $R = 1$, and for $J_{\boldsymbol{\varphi}} := J(\boldsymbol{\varphi}, \mathbf{u})$ are $\mathbf{Q}_{\boldsymbol{\varphi}} = \mathbf{Q}$ and $R_{\boldsymbol{\varphi}} = 4R$. The choice for $R_{\boldsymbol{\varphi}}$ ensures a fair comparison by enforcing the same applied energy input for all methods.

Performance results are summarized in figure 9. It is also possible to combine KRONIC with MPC allowing for more general objective functions. Then, the control could be formulated in terms of $J_{\mathbf{x}}$ by computing the inverse $\boldsymbol{\varphi}^{-1} : \mathbb{R}^r \to \mathbb{R}^n$ if it exists or estimating $\mathbf{x}$ from $\boldsymbol{\varphi}$ using, e.g. multidimensional scaling as in [57]. Control in Koopman intrinsic coordinates allows one to discard uncontrollable, unstable directions, for which standard control toolboxes such as Matlab's `lqr` fail. Note that feedback linearization fails in this case too: The control law is of the form $u_{\mathrm{FL}} = x_1^{-1}\mathbf{C}_{\mathrm{FL}}\mathbf{x}$. As the system approaches the origin, the control input becomes unboundedly large.

7. Example: hamiltonian energy control

Conserved quantities, such as the Hamiltonian, are Koopman eigenfunctions associated with the eigenvalue $\lambda = 0$. Hamiltonian systems represent a special class of systems for which we can easily discover a Koopman eigenfunction directly from data.

The dynamics of a Hamiltonian system are governed by

$$\frac{\mathrm{d}}{\mathrm{d}t}\mathbf{q} = \frac{\partial\mathcal{H}}{\partial\mathbf{p}}, \quad \frac{\mathrm{d}}{\mathrm{d}t}\mathbf{p} = -\frac{\partial\mathcal{H}}{\partial\mathbf{q}}, \tag{57}$$

where $\mathbf{q}$ and $\mathbf{p}$ are the generalized state and momenta vectors, respectively. The Hamiltonian $\mathcal{H} = \mathcal{H}(\mathbf{q}, \mathbf{p})$ considered here is time-independent, representing the conserved energy in the system. Trajectories of the system evolve on constant energy hypersurfaces $\{(\mathbf{q}, \mathbf{p}) : \mathcal{H}(\mathbf{q}, \mathbf{p}) = \mathcal{E}\}$, which may be interpreted as oscillatory modes. Thus, energy level stabilization is a form of oscillation control and corresponds to stabilizing invariant manifolds in phase space. Also nonlinear fixed point stabilization may correspond to stabilizing a particular value of the Hamiltonian energy.

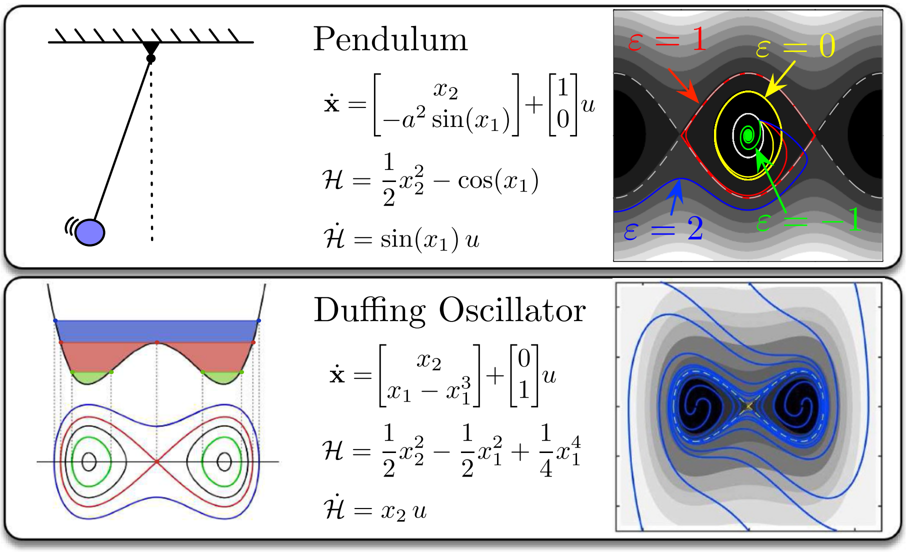

Figure 10. KRONIC demonstrated for several Hamiltonian systems.

Consider the nonlinear, control-affine Hamiltonian system $\frac{\mathrm{d}}{\mathrm{d}t}\mathbf{x} = \boldsymbol{f}(\mathbf{x}) + \mathbf{B}\mathbf{u}$ where $\boldsymbol{f} = [\partial\mathcal{H}/\partial\mathbf{p} - \partial\mathcal{H}/\partial\mathbf{q}]^T$, with state vector $\mathbf{x} = [\mathbf{q}\ \mathbf{p}]^T \in \mathbb{R}^n$, multi-channel input vector $\mathbf{u} \in \mathbb{R}^q$, and constant control matrix $\mathbf{B} \in \mathbb{R}^{n\times q}$. We may develop the control directly for the eigenfunction equation

$$\frac{\mathrm{d}}{\mathrm{d}t}\varphi = 0\cdot\varphi + \nabla_{\mathbf{x}}\varphi\cdot\mathbf{B}\mathbf{u} := \mathbf{B}_\varphi\mathbf{u}, \tag{58}$$

where $\varphi = \mathcal{H}$. This equation also represents the energy conservation law of the system: A change in the energy, i.e. the Hamiltonian, corresponds to the external supplied work via $\mathbf{u}$. The infinite-time horizon cost function to be minimized is $J = \lim_{t\to\infty}\frac{1}{2}\int_0^t Q\left(\mathcal{H}(\mathbf{x}(t))\right)^2 + \mathbf{u}^T(t)\mathbf{R}\mathbf{u}(t)\,\mathrm{d}t$ with scalar Q penalizing energy deviations and $\mathbf{R}$ penalizing the cost expenditure. Assuming a single input u, the control law is given by $u = -\mathrm{sign}(B_{\mathcal{H}})\sqrt{Q/R}\mathcal{H}(\mathbf{x})$ feeding back the current energy level $\mathcal{H}(\mathbf{x})$. The ratio Q/R determines how aggressive the controller is. A more aggressive controller, with $Q > R$, leads to a faster but also more costly convergence to the desired state, and vice versa. For the specific case $Q = R$, the control law reduces further to $u = -\mathrm{sign}(B_{\mathcal{H}})\mathcal{H}(\mathbf{x})$. Note that this feedback control law is linear in the Hamiltonian function, but nonlinear in the state $\mathbf{x}$. In the following, we demonstrate the control approach for several Hamiltonian systems by solving the SDRE; an overview is provided in figure 10, where colored curves represent Koopman controlled trajectories. We assume $Q = R = 1$ for all examples.

7.1. Frictionless pendulum

A frictionless pendulum given by a negative cosine potential $V(x) = -\cos(x_1)$ is steered towards different energy levels $\mathcal{H}^{\mathrm{REF}}(\mathbf{x}) = \mathcal{E}\,\forall\mathbf{x}$, $\mathcal{E} \in \{-1, 0, 1, 2\}$, with feedback law $u = -C(\mathcal{H}(\mathbf{x}) - \mathcal{H}^{\mathrm{REF}}) = -C(\mathcal{H}(\mathbf{x}) - \mathcal{E})$. Minimizing the Hamiltonian drives the system to the equilibrium point at the origin with $\mathcal{E} = -1$ (green curve in figure 10). Koopman control has improved performance over an LQR controller based on linearized dynamics near the center.

We further compare the controller resulting from solving the state-dependent Riccati equation with an energy-based control (EC) [7], which is developed from physical considerations:

$$\mathrm{SDRE}: \mathbf{B} = \begin{bmatrix} 0 \\ 1 \end{bmatrix}, \quad \dot{\mathcal{H}} = x_2 u, \quad u = -\mathrm{sign}(x_2)(\mathcal{H}(\mathbf{x}) - \mathcal{E}) \tag{59a}$$

$$\mathrm{EC}: \mathbf{B} = \begin{bmatrix} 0 \\ -\cos(x_1) \end{bmatrix}, \ \dot{\mathcal{H}} = -x_2\cos(x_1)u, \ u = -\mathrm{sign}(-x_2\cos(x_1))(\mathcal{H}(\mathbf{x}) - \mathcal{E}). \tag{59b}$$

If the functional representation of the Koopman eigenfunction, or specifically here the Hamiltonian energy function, is identified from data as in KRONIC, the feedback gain can be precomputed and does not need to

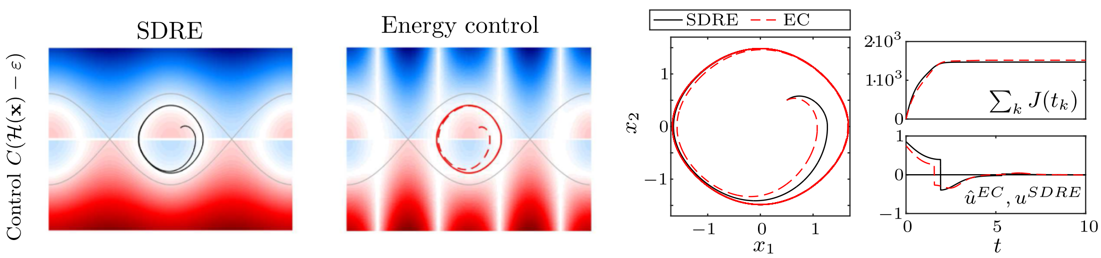

Figure 11. Comparison of the energy control control strategy [7] and SDRE for the pendulum with $\varepsilon = 0.1$. The color coding in the phase plots depicts the respective state-dependent control.

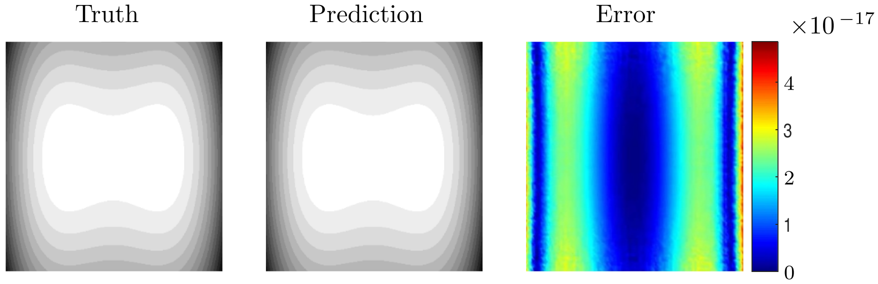

Figure 12. Prediction over the state space and error using the discovered Hamiltonian for the Duffing system trained on a single trajectory.

be computed on-line. In figure 11, the state-dependent feedback law is shown for both controllers as color-coded phase plots, where negative values are depicted by blue and positive values by red. The extrema are identical. The control input from the EC controller is here slightly modified compared with (59*b*) by moving the term $-\cos(x_1)$ into u itself. Then the effective control and performance are displayed in terms of $\hat{u} = -\cos(x_1)u$ for a fair comparison; otherwise, the EC controller would appear less performing. The pendulum dynamics are locally controllable as long as u does not vanish, which is achieved if $x_1 \neq \pi/2$ and $x_2 \neq 0$ for the EC controller and if $x_2 \neq 0$ for the SDRE controller. Both controllers yield a bang-bang strategy and successfully steer the system to the desired energy level, though the SDRE controller is performing slightly better.

7.2. Duffing system

Certain damped or forced oscillators are described by the Duffing equation (figure 10). The system is steered towards the energy level $\mathcal{E} = 0$, which corresponds to the separatrix cycle (yellow dashed lines) yielding a periodic solution. The origin is a saddle point leading to a homoclinic orbit defined by $x_2^* = \pm x_1^* \sqrt{1 - 1(x_1^*)^2/2}$ for $x_1^* \leqslant \pm\sqrt{2}$. It is possible to stabilize the center fixed points by commanding a lower reference energy; however, because of symmetry in the system, both fixed points are indistinguishable in eigenfunction coordinates. This illustrates a fundamental *uncertainty* associated with Koopman eigenfunction control.

For the eigenvalue $\lambda = 0$, (42) becomes $-\boldsymbol{\Gamma}(\mathbf{X}, \dot{\mathbf{X}})\boldsymbol{\xi} = \mathbf{0}$, and hence a sparse $\boldsymbol{\xi}$ is sought in the null-space of $-\boldsymbol{\Gamma}(\mathbf{X}, \dot{\mathbf{X}})$. Polynomials up to fourth order are employed to construct a library of candidate functions in (40) and (41). A single time series for $t \in [0, 10]$ with time step $\Delta t = 0.001$ starting at the initial state $\mathbf{x}_0 = [0, \ -2.8]^T$ is collected. Thus, each row in (40) and (41) corresponds to a time instant of the trajectory. The prediction and associated error of the identified eigenfunction are displayed in figure 12. Here, the energy is predicted over the full state space using the identified eigenfunction, the Hamiltonian energy function, which is trained from a single trajectory. The magnitude of the error is very small of $\mathcal{O}(10^{-17})$. However, the eigenfunction evaluate on a trajectory would oscillate with a tiny amplitude around the true energy level.

The error of the regression problem, the computational time for identifying the eigenfunction, and the control performance (steering towards $\mathcal{E} = 0$) for an increasing number of measurements in the estimation step are displayed in figure 13. The identified Koopman eigenfunction with $\lambda = 0$ from 1792 measurements (kink in figure 13(b)) is $\varphi(\mathbf{x}) = [x_1^2 \ x_2^2 \ x_1^4]\,[-\frac{2}{3} \ \frac{2}{3} \ \frac{1}{3}]^T$ with error $\mathcal{O}(10^{-8})$. This eigenfunction represents a perfect recovery of the Hamiltonian up to a scaling, as a Hamiltonian multiplied by a constant scalar is also a

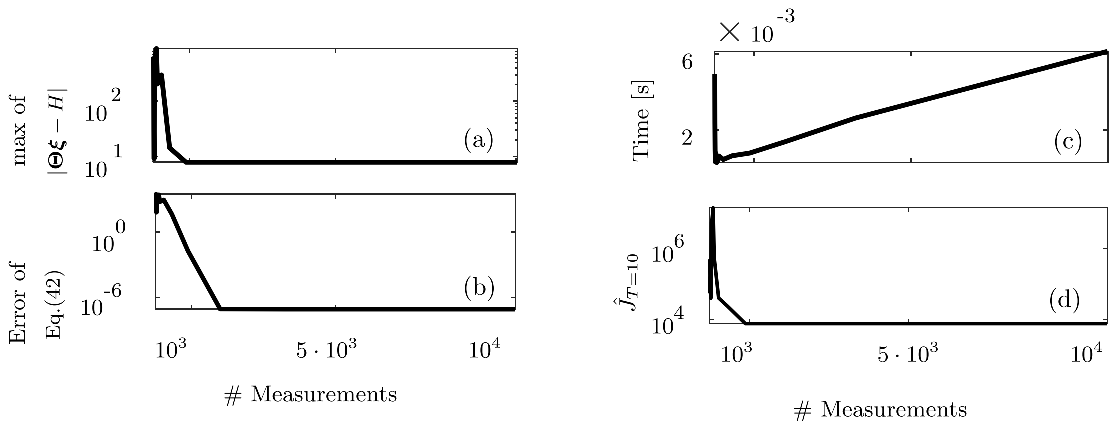

Figure 13. Dependency in increasing number of measurements for the Duffing system: (a) error in the Koopman eigenfunction, (b) error in (42) with estimated $\boldsymbol{\xi}$, (c) computational time to solve for $\boldsymbol{\xi}$ in (42), and (d) cumulative control performance $\hat{J}$ over $T = 10$ time units.

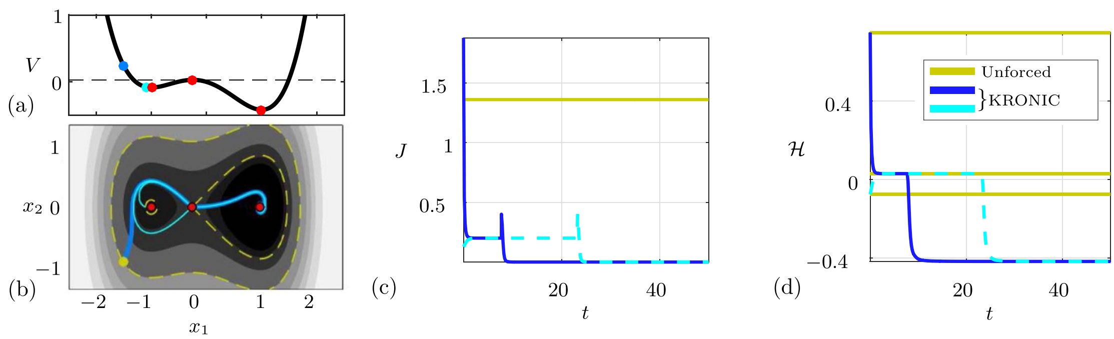

Figure 14. Switching control strategy based on KRONIC and the homoclinic orbit to jump between wells: (a) potential function $V(x_1)$ showing initial conditions (blue and cyan) and extrema (red), (b) phase plot with unforced (yellow) and controlled trajectories (blue and cyan), (c) instantaneous cost function and (d) total energy.

conserved quantity. Using a larger time step of $\Delta t = 0.05$, 56 measurements are sufficient to learn the eigenfunction with error $\mathcal{O}(10^{-6})$.

8. Example: basin hopping in a double well

A Koopman eigenfunction represents a topography over the state; e.g. the Hamiltonian function depicts the energy landscape of the system. Trajectory control of a set of particles based on a single Koopman eigenfunction is driven by the difference between the current and desired value in this topography. While the Koopman eigenfunction is a global, linear representation of the system, the control of the particle is local, e.g. by solving a suboptimal SDRE. This is illustrated for a particle in an asymmetric double potential $V(x_1) = \frac{1}{4}x_1^4 - \frac{1}{2}x_1^2 - \frac{a}{3}x_1^3 + ax_1$ with $a = -0.25$ (figure 14(a)). The Hamiltonian is $\mathcal{H} = x_2^2/2 + V(x_1)$ and the dynamics are

$$\frac{\mathrm{d}}{\mathrm{d}t}\begin{bmatrix} x_1 \\ x_2 \end{bmatrix} = \begin{bmatrix} x_2 \\ -x_1^3 + ax_1^2 + x_1 - a \end{bmatrix} + \begin{bmatrix} 1 & 0 \\ 0 & 1 \end{bmatrix}\mathbf{u}. \tag{60}$$

For an initial condition in the left well (blue dots in figure 14(a)) the controller will fail to steer the state to the fixed point $\mathbf{x}^* = [1\ 0]^T$ in the center of the right well as the trajectory will become trapped in the bottom of the left well. Instead, the controller must first increase the energy level to the saddle transition, and after the trajectory passes to the right basin, the energy can be decreased further.

We propose a switching control strategy that exploits the Koopman eigenfunctions to transport particles between basins of different heights associated with different fixed points. In particular, the following control strategy steers particles from the left to the right basin:

$$\mathbf{u} = \begin{cases} -\mathbf{C}(\mathbf{x})(\mathcal{H}(\mathbf{x}) - \mathcal{H}([a,0])) & \text{if } \mathcal{H}(\mathbf{x}) < \mathcal{H}([a,1]), \\ 0 & \text{if } \mathcal{H}(\mathbf{x}) = \mathcal{H}([a,1]) \text{and } x_1 \leqslant a, \\ -\mathbf{C}(\mathbf{x})(\mathcal{H}(\mathbf{x}) - \mathcal{H}([1,0])) & \text{if } x_1 > a. \end{cases}$$

A particle on an energy level lower than $\mathcal{H}([a,1])$, associated with the saddle point, is first steered onto a trajectory with slightly higher energy than the homoclinic orbit connecting the two basins. On this orbit, control is turned off and the particle travels to the right well exploiting the intrinsic system dynamics. As soon as it passes the saddle point, control is turned on again directing it to the lowest energy level $\mathcal{H}([1,0])$ at the desired fixed point. The controller is demonstrated for two initial conditions, as shown in figures 14(b)–(d), driving both to the desired energy level.

This controller can be fully derived from data: First, relevant Koopman eigenfunctions can be identified from data, as shown in section 5. By analyzing roots and extrema of the eigenfunction corresponding to $\lambda = 0$, equilibrium and saddle points can be identified. The homoclinic and heteroclinic orbits associated with the saddles can be used as natural transit paths between basins. In each basin, eigenfunction control drives the system to the desired state. Future applications for this control strategy include space mission design and multi-stable systems such as proteins.

9. Example: double gyre flow

We now consider a high-dimensional, spatially evolving, non-autonomous dynamical system, with time-dependent Koopman eigenfunctions. The periodically driven double gyre flow models the transport between convection cells in the Rayleigh-Bénard flow due to lateral oscillations, yielding a simple model for the gulf stream ocean front [104]. We employ here the same parameters as in Shadden *et al*'s seminal work on Lagrangian coherent structures [102].

The time-dependent stream function is

$$\Psi(x,y,t) = A\sin(\pi f(x,t))\sin(\pi y) \tag{61a}$$

$$\text{with} \quad f(x,t) = \varepsilon\sin(\omega t)x^2 + (1 - 2\varepsilon\sin(\omega t))x \tag{61b}$$

with $A = 0.25$, $\omega = 2\pi$, and $\varepsilon = 0.25$ on a periodic domain $[0,2]\times[0,1]$. The velocity field $\mathbf{v} = [v_x\ v_y]^T$ is given by $v_x = -\frac{\partial\Psi}{\partial y}$ and $v_y = \frac{\partial\Psi}{\partial x}$.

The control objective is to steer an ensemble of trajectories to a level set of the stream function. This can be interpreted as the control of an ensemble of active drifters or autonomous gliders in the ocean, which drift due to hydrodynamic forces associated with v_x and v_y. The dynamics of the ith drifter are $\frac{\mathrm{d}}{\mathrm{d}t}\left[\begin{smallmatrix} x_i \\ y_i \end{smallmatrix}\right] = \left[\begin{smallmatrix} v_x + \gamma_i\sin(\theta_i) \\ v_y + \gamma_i\cos(\theta_i) \end{smallmatrix}\right] = \left[\begin{smallmatrix} v_x \\ v_y \end{smallmatrix}\right] + \left[\begin{smallmatrix} 1 & 0 \\ 0 & 1 \end{smallmatrix}\right]\mathbf{u}$.

For the autonomous and unforced flow with $\varepsilon = 0$, the stream function is a Koopman eigenfunction associated with the eigenvalue $\lambda = 0$. The forced system becomes

$$\frac{\mathrm{d}}{\mathrm{d}t}\Psi(x,y) = \underbrace{\begin{bmatrix} \frac{\partial\Psi}{\partial x} & \frac{\partial\Psi}{\partial y} \end{bmatrix} \cdot \begin{bmatrix} -\frac{\partial\Psi}{\partial y} \\ \frac{\partial\Psi}{\partial x} \end{bmatrix}}_{=0} + \underbrace{\begin{bmatrix} \frac{\partial\Psi}{\partial x} & \frac{\partial\Psi}{\partial y} \end{bmatrix} \cdot \mathbf{B}}_{\mathbf{B}_\Psi(x,y)}\mathbf{u}. \tag{62}$$

Without control, the stream function Ψ is conserved, as it is the negative of the Hamiltonian. The particles follow streamlines, which are isolines of the stream function.

In the non-integrable case, with $\varepsilon > 0$, the total derivative of the stream function is given by

$$\frac{\mathrm{d}}{\mathrm{d}t}\Psi(x,y,t) = A_\Psi(x,y,t)\Psi + \mathbf{B}_\Psi(x,y,t)\,\mathbf{u} \tag{63}$$

where the vanishing term in (62) is not displayed. The first term in (63) arises from the time derivative $\frac{\partial}{\partial t}\Psi(x,y,t)$ and is reformulated into a linear-like structure in Ψ: $\partial\Psi/\partial t = A\pi\cos(\pi f(x,t))\sin(\pi y)(\partial f/\partial t) = \pi\tan^{-1}(\pi f(x,t))(\partial f/\partial t)\Psi = A_\Psi\Psi$. The second term is the time-dependent analogue of the corresponding term in (62).

For both cases, $\varepsilon = 0$ and $\varepsilon > 0$, a controller is developed for the stream function. The control is then applied to an ensemble of drifters to steer them towards the level set $\Psi = 0.2$. As in the previous examples a quadratic cost function with $Q = 1$ and $\mathbf{R} = \left(\begin{smallmatrix} 1 & 0 \\ 0 & 1 \end{smallmatrix}\right)$ is considered. In both cases, $\mathbf{B}_\Psi$ and A_Ψ depend on the state, and for $\varepsilon > 0$ also on time. Thus, the state-dependent Riccati equation is solved at each point in space and time. The controller successfully drives an ensemble of drifters distributed over the domain to the

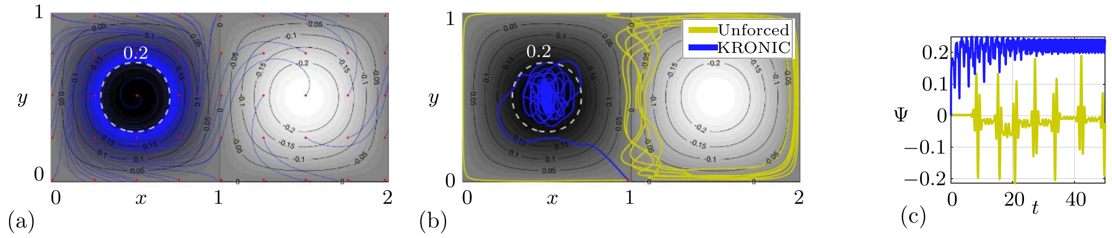

Figure 15. Controlled double gyre flow: (a) autonomous with $\varepsilon = 0$ steering an ensemble of drifters (initial condition depicted by red dots) to the level $\Psi = 0.2$, (b) a single drifter trajectory (unforced and controlled) in the non-autonomous double gyre flow with $\varepsilon = 0.25$, and (c) corresponding stream function values.

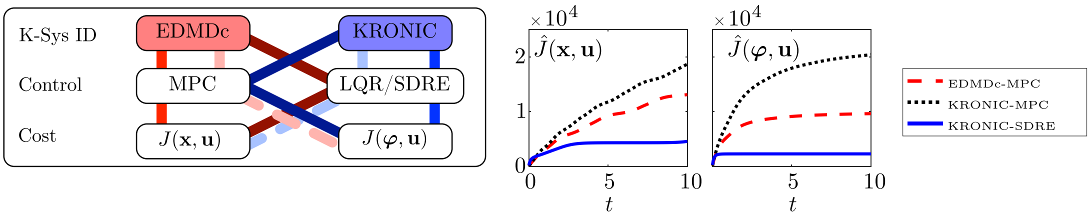

Figure 16. Comparison of Koopman system identification methods for control demonstrated for the Duffing system. Here, EDMDc-MPC requires knowledge of the Koopman eigenfunction. The employed weights are $Q_H = 1$ and $R = 1$ for $J_{\boldsymbol{\varphi}}$, and $\mathbf{Q} = \texttt{eye}(2)$ and $R = 1$ for $J_{\mathbf{x}}$ (instantaneous cumulative costs are shown here). The prediction and control horizon for MPC is in both cases $N = 5$.

desired level, as shown in figure 15(a). Trajectories are integrated using a 4th-order Runge-Kutta scheme from $t \in [0, 10]$. Example trajectories of the non-autonomous system, with and without control, are presented in figures 15(b) and (c).

Note that in the non-autonomous case, the reference isocurve $\Psi_{\mathrm{REF}} = 0.2$ (white dashed in figure 15(b)) oscillates from left to right while being periodically compressed and expanded in x-direction. The particles follow the moving isocurve resulting in a small oscillation around the desired value (see figure 15(c)).

Koopman eigenfunction control can be interpreted in two ways: (a) applying local control to internally driven swimmers or particles in an external field such as a fluid flow or magnetic field; or (b) driving the external field in which the swimmers or particles drift. In the latter case, control drives the amplitude of the stream function at each point to the desired value. For the double gyre flow with a constrained spatial domain, the spatially distributed gain may be precomputed.

10. Discussion and conclusions

In summary, we extend the Koopman operator formalism to include actuation, and demonstrate how a nonlinear control problem may be converted into a bilinear control problem in eigenfunction coordinates. Next, we have presented a data-driven framework to identify leading eigenfunctions of the Koopman operator and sparsity-promoting extensions to EDMD. We find that lightly damped or undamped eigenfunctions may be accurately approximated from data via regression, as these eigenfunctions correspond to persistent phenomena, such as conserved quantities. Moreover, these are often the structures that we seek to control, since they affect long-time behavior. We have demonstrated the efficacy of this new data-driven control architecture on a number of nonlinear systems, including Hamiltonian systems and a challenging high-dimensional ocean mixing model. These results suggest that identifying and controlling Koopman eigenfunctions may enable significant progress towards the ultimate goal of a universal data-driven nonlinear control strategy.

Finite-dimensional approximations of the Koopman operator are typically obtained as its projection onto a specified basis, which may suffer from a well-known closure issue. The matrix $\mathbf{K}$ is usually large, as the state is lifted to a high-dimensional space, and the resulting model rarely closes and spurious eigenfunctions may appear. Building on EDMD, we construct a reduced-order model using validated Koopman eigenfunctions, so that the resulting model will be *closed by design*. Both KRONIC and EDMD with control [64] provide Koopman-based system identification that can be leveraged for model-based control, such as MPC or LQR, as shown in figure 16. However, there are a number of key differences: (a) KRONIC directly identifies Koopman eigenfunctions, while EDMDc approximates the Koopman operator restricted to a high-dimensional span of observables. (b) EDMD augments the state vector with nonlinear measurements, increasing the dimension of the system. In contrast, KRONIC yields a reduced-order model in terms of a few Koopman eigenfunctions. (c) Control is incorporated in EDMDc as an approximated affine linear term. KRONIC derives an expression for how eigenfunctions are affected by control through the generator equation. However, this may render the control term bilinear (nonlinear in the state). (d) The cost function for EDMDc is defined in the state or measurement space, while KRONIC defines the cost in eigenfunctions; note that these cost functions are not always transferable. (e) Finally, KRONIC readily admits more complicated solutions, such as limit cycle stabilization, as these correspond to level sets of the eigenfunctions.

As with previous studies, this work further cements the importance of accurate identification and representation of Koopman eigenfunctions. Future work will continue to develop algorithms to extract approximate eigenfunctions from data, and it is likely that these efforts will benefit from advances in machine learning. In addition, there is a fundamental uncertainty principle in representing Koopman eigenfunctions, as these eigenfunctions may themselves be irrepresentable, as are the long-time flow maps for chaotic systems. Instead of seeking perfect Koopman eigenfunctions, which may not be attainable, it will be important to incorporate uncertainty quantification into the data-driven Koopman framework. Model uncertainties may then be managed with robust control.

The present work also highlights an important choice of perspective when working with Koopman approximations. Generally, Koopman eigenfunctions are global objects, such as the Hamiltonian energy function. Although a global, linear representation of the dynamics is appealing, there is also information that is stripped from these representations. For example, in the case of the Hamiltonian eigenfunction, information about specific fixed points and spatial locations are folded into a single scalar energy. If the Hamiltonian is viewed as a topography over the phase space, then this eigenfunction only carries information about the *altitude*, and not the *location*. In contrast, Lan and Mezić [71] show that it is possible to extend the Hartman–Grobman theorem to the entire basin of attraction of certain fixed points and periodic orbits, providing a *local* linear embedding of the dynamics. Connecting these perspectives will continue to yield interesting and important advances in Koopman theory. In addition, there are known connections between the eigenvalues of geometric structures in phase space and the spectrum of the Koopman operator [82]. This knowledge may guide the accurate identification of Koopman eigenfunctions.

Formulating control in terms of Koopman eigenfunctions requires a change of perspective as the control objective may now be defined in eigenfunctions coordinates. Eigenfunctions characterize, e.g. geometric properties of the system, such as fixed points and limit cycles, as particular level sets, and the control objective can be equivalently formulated to steer the system towards these objects. Further, particular eigenfunctions represent coherent structures, i.e. persistent features of the system, which have been targeted in control for a long time. However, the specific selection of eigenfunctions to control and their interpretation regarding specific control goals remains an open problem. Nevertheless, it may still be possible to formulate the control in the original state space, e.g. by incorporating the state as observables, modifying the state weight matrix appropriately, or by learning an approximation of the inverse mapping [57], which can be more easily incorporated in the context of model predictive control. This also motivates additional work to understand how controllability and observability in these coordinates relate to properties of the nonlinear system. The degree of observability and controllability will generally vary with different eigenfunctions, so that it may be possible to obtain balanced realizations. Moreover, classic results, such as the PBH test, indicate that multi-channel actuation may be necessary to simultaneously control different eigenfunctions corresponding to the same eigenvalue, such as the Hamiltonian energy and conserved angular momentum. The additional degrees of freedom arising from multi-channel inputs can also be used for eigenstructure assignment to shape Koopman eigenfunctions [49]. Thus, actuation may modify both the shape of coherent structures (i.e. Koopman modes associated with a particular eigenfunction) and their time dynamics. It may also be possible to use Koopman linear embeddings to optimize sensor and actuator placement for nonlinear systems.

Finally, as undamped or lightly damped eigenfunctions correspond to conserved or nearly conserved quantities, there are many potential applications of the proposed control strategy. For example, symmetries give rise to other conserved quantities, which will likewise yield new Koopman eigenfunctions. In many physical systems, simultaneously controlling the system energy and angular momentum may be an important goal. Much of the present work was formulated with the problem of space mission design in mind. Energy efficient transport throughout the Solar System has long driven advances in theoretical and computational dynamical systems, and may stand to benefit from control based on Koopman eigenfunctions. More generally, there is a broad range of applications that stand to benefit from improved nonlinear control, include self-driving cars, the control of turbulence, suppressing the spread of disease, stabilizing financial markets, human machine interfaces, prosthetics and rehabilitation, and the treatment of neurological disorders, to name only a few.

Data availability statement

The data that support the findings of this study are openly available at the following URL/DOI: https://github.com/eurika-kaiser/KRONIC.

Acknowledgments

EK acknowledges funding by the Moore/Sloan foundation, the Washington Research Foundation, and the eScience Institute. S L B and J N K acknowledge support from the Defense Advanced Research Projects Agency (DARPA contract HR011-16-C-0016) and the UW Engineering Data Science Institute, NSF HDR award #1934292. S L B acknowledges support from the Army Research Office (W911NF-17-1-0306) and the Air Force Office of Scientific Research (FA9550-16-1-0650). J N K acknowledges support from the Air Force Office of Scientific Research (FA9550-15-1-0385). The authors gratefully acknowledge many valuable discussions with Josh Proctor about Koopman theory and extensions to control. We would also like to acknowledge Igor Mezić, Maria Fonoberova, Bernd Noack, Clancy Rowley, Sam Taira, and Lionel Mathelin.

Appendix A. Optimal control

We begin by formulating optimal control for the full nonlinear system in (16). This procedure then simplifies considerably for linearly factorizable or linear dynamics, motivating Koopman embeddings.

A.1. Hamilton–Jacobi–Bellman equation

A nonlinear optimal control formulation for the system in (16) can be established using dynamic programming [15]. This relies on Bellman's principle of optimality [13], stating that an optimal trajectory remains optimal when the problem is initialized at intermediate steps, and leads to the Hamilton–Jacobi–Bellman (HJB) equation [12]:

$$0 = \inf_{\mathbf{u}} \{L(\mathbf{x},\mathbf{u}) + \nabla_{\mathbf{x}} J^* \cdot \boldsymbol{f}(\mathbf{x},\mathbf{u})\} = \inf_{\mathbf{u}} H(\mathbf{x}, \nabla_{\mathbf{x}} J^*, \mathbf{u})\,. \tag{A1}$$

If the HJB equation (A1) has a continuously differentiable, positive definite solution $J^*(\mathbf{x})$ [15], also referred to as an optimal value function, then the optimal control law is

$$\mathbf{u}^* = \arg\min_{\mathbf{u}} H\left(\mathbf{x}^*, \frac{\partial J^*}{\partial x}, \mathbf{u}\right). \tag{A2}$$

The solution is a state-feedback control law, i.e. a *closed-loop* controller, which is optimal for any initial condition and solved for all states at once. Solving this nonlinear PDE is computationally challenging and only feasible for low-dimensional problems. If solved, however, the HJB equation provides a global solution to the optimal control problem.

A.2. Euler–Lagrange equations

An alternative approach searches for the optimal trajectory under certain constraints using a variational argument and Pontryagin's minimum (or maximum) principle [91]. Here, a small variation around an optimal trajectory is considered, for which the change in cost shall vanish. The sequence of control inputs that solves this problem, constrained by the state dynamics (16), constitutes the optimal control. However, the Euler–Lagrange equations provide only necessary, but not sufficient, conditions, so that the solution may only converge to a local minimum and the control is generally not optimal in practice.

Similar to (A1), a Lagrange-type expression is formulated for the control Hamiltonian $H(\mathbf{x},\mathbf{u},\mathbf{z}) := L(\mathbf{x},\mathbf{u}) + \mathbf{z}^T\boldsymbol{f}(\mathbf{x},\mathbf{u})$, where $\mathbf{z}$ is referred to as Lagrange multiplier, co-state or adjoint variable. A necessary condition is the minimization of the control Hamiltonian (i.e. Pontryagin's minimum principle), leading to the following set of coupled ordinary differential equations:

$$\dot{\mathbf{x}} = \frac{\partial H^T}{\partial \mathbf{z}}(\mathbf{x},\mathbf{u}^*,\mathbf{z}) = \boldsymbol{f}(\mathbf{x},\mathbf{u}) \tag{A3a}$$

$$\dot{\mathbf{z}} = -\frac{\partial H^T}{\partial \mathbf{x}}(\mathbf{x},\mathbf{u}^*,\mathbf{z}) \tag{A3b}$$

with stationarity condition $\frac{\partial H^T}{\partial \mathbf{u}}(\mathbf{x},\mathbf{u}^*,\mathbf{z}) = 0$ and transversality boundary conditions $\mathbf{x}(0) = \mathbf{x}_0$ and $\lim_{T\to\infty} \mathbf{z}(T) = \mathbf{0}$. Then, the optimal control is given by

$$\mathbf{u}^* = \arg\min_{\mathbf{u}} H(\mathbf{x},\mathbf{u},\mathbf{z}). \tag{A4}$$

If $L(\cdot)$ and $\boldsymbol{f}(\mathbf{x}(\cdot),\mathbf{u}(\cdot))$ are concave, then the necessary condition is also sufficient and any path that satisfies these conditions also solves the optimal control problem.

The Euler–Lagrange equations (A3a) lead to an optimal *open-loop* control: The control $\mathbf{u}^*$ point-wise minimizes the control Hamiltonian $H(\mathbf{x}^*(t),\mathbf{u},\mathbf{z}^*(t))$. This two-point boundary value (TPBV) problem is solvable for higher-dimensional problems in contrast to the HJB equation. However, in practice, only a local minimum is found. For systems with a high number of degrees of freedom, such as fluid flows, expensive direct and adjoint simulations render this approach infeasible, instead motivating the use of reduced-order models.

A.3. Linear or factorized systems

The control problem above simplifies considerably for linear systems of the form

$$\frac{\mathrm{d}}{\mathrm{d}t}\mathbf{x}(t) = \mathbf{A}\mathbf{x} + \mathbf{B}\mathbf{u}, \quad \mathbf{x}(0) = \mathbf{x}_0. \tag{A5}$$

Using ansatz $\mathbf{z} = \mathbf{P}\mathbf{x}$ for the co-state, the optimal control is given by

$$\mathbf{u} = -\mathbf{R}^{-1}\mathbf{B}^T\mathbf{z} = -\mathbf{R}^{-1}\mathbf{B}^T\mathbf{P}\mathbf{x}, \tag{A6}$$

with constant gain $\mathbf{C} = \mathbf{R}^{-1}\mathbf{B}^T\mathbf{P}$ and where the positive semi-definite matrix $\mathbf{P} \in \mathbb{R}^{n\times n}$ is the solution to the algebraic Riccati equation (ARE) [106]:

$$\mathbf{Q} + \mathbf{P}\mathbf{A} + \mathbf{A}^T\mathbf{P} - \mathbf{P}\mathbf{B}\mathbf{R}^{-1}\mathbf{B}^T\mathbf{P} = \mathbf{0}. \tag{A7}$$

For this special case, referred to as the linear quadratic regulator (LQR), the Euler–Lagrange equations and the HJB equation lead to the same solution, using a quadratic ansatz for co-state and value function. The ARE (A6) can be solved upfront and yields a global state-feedback control law. This simplicity motivates efforts to find linear representations for nonlinear systems and explains why nonlinear embeddings via Koopman operator theory are so appealing.

For later reference, we point out an extension of LQR to control-affine, nonlinear systems by factoring the governing equations into a linear-like structure, as in (A5), where the state transition matrix and actuation matrix become state-dependent:

$$\frac{\mathrm{d}}{\mathrm{d}t}\mathbf{x}(t) = \mathbf{A}(\mathbf{x})\mathbf{x} + \mathbf{B}(\mathbf{x})\mathbf{u}, \quad \mathbf{x}(0) = \mathbf{x}_0. \tag{A8}$$

For these systems, it is common to solve the ARE point-wise, i.e. at each point $\mathbf{x}$ in time, leading to the state-dependent Ricatti (SDRE) equation [89]

$$\mathbf{Q} + \mathbf{P}\mathbf{A}(\mathbf{x}) + \mathbf{A}^T(\mathbf{x})\mathbf{P} - \mathbf{P}\mathbf{B}(\mathbf{x})\mathbf{R}^{-1}\mathbf{B}^T(\mathbf{x})\mathbf{P} = \mathbf{0} \tag{A9}$$

where the weight matrices $\mathbf{Q}$ and $\mathbf{R}$ may also be state dependent. In contrast to the ARE, which can be pre-computed off-line, the SDRE is solved on-line at each $\mathbf{x}$. The required computational power and memory during the on-line phase may render it infeasible for high-dimensional systems. The SDRE generalizes LQR for nonlinear systems, retaining a simple implementation and often yielding near optimal controllers [30]. We refer to [29, 31] for a review on the SDRE and related discussions, e.g. on controllability and stability.

Appendix B. Effect of misrepresentation of eigenfunctions

We examine the effect of an error in the representation of a Koopman eigenfunction on the closed-loop dynamics based on (33) and provide an upper error bound. We consider the following cost function

$$J = \int Q\varphi^2(\mathbf{x}) + \mathbf{R}\mathbf{u}^2\,\mathrm{d}t \tag{B1}$$

where a single eigenfunction $\varphi(\mathbf{x})$ is to be controlled and with positive weights Q and $\mathbf{R}$. Assuming a control-affine system $\dot{\mathbf{x}} = \mathbf{f}(\mathbf{x}) + \mathbf{B}(\mathbf{x})\mathbf{u}$, the eigenfunction satisfies

$$\dot{\varphi}(\mathbf{x}) = \lambda\varphi(\mathbf{x}) + \mathbf{C}(\mathbf{x})u \tag{B2}$$

with $\mathbf{C}(\mathbf{x}) := \nabla\varphi(\mathbf{x})\cdot\mathbf{B}(\mathbf{x})$. Here, φ is the Koopman eigenfunction associated with the autonomous dynamics satisfying $\dot{\varphi} = \nabla\varphi(\mathbf{x})\cdot\mathbf{f}(\mathbf{x}) = \lambda\varphi(\mathbf{x})$. We assume full-state measurements $\mathbf{x}$ are available and knowledge of how the control affects these measurements $\mathbf{B}(\mathbf{x})$. Thus, we do not have to represent the control term $\mathbf{C}(\mathbf{x})$ in terms of eigenfunctions but can evaluate it exactly given the current measurement $\mathbf{x}$ and knowledge of $\varphi(\mathbf{x})$. Solving the scalar Riccati equation (33) analytically yields

$$P = \frac{1}{\mathbf{C}(\mathbf{x})\mathbf{R}^{-1}\mathbf{C}^T(\mathbf{x})}\left(\lambda + \sqrt{\lambda^2 + Q\mathbf{C}(\mathbf{x})\mathbf{R}^{-1}\mathbf{C}^T(\mathbf{x})}\right). \tag{B3}$$

The feedback control is then given by

$$\mathbf{u} = -\mathbf{R}^{-1}\mathbf{C}^T P\varphi = -\frac{\mathbf{R}^{-1}\mathbf{C}^T(\mathbf{x})}{\mathbf{C}(\mathbf{x})\mathbf{R}^{-1}\mathbf{C}^T(\mathbf{x})}\left(\lambda + \sqrt{\lambda^2 + Q\mathbf{C}(\mathbf{x})\mathbf{R}^{-1}\mathbf{C}^T(\mathbf{x})}\right)\varphi(\mathbf{x}) \tag{B4}$$

and the resulting closed-loop dynamics are

$$\dot{\varphi}(\mathbf{x}) = -\sqrt{\lambda^2 + Q\mathbf{C}(\mathbf{x})\mathbf{R}^{-1}\mathbf{C}^T(\mathbf{x})}\varphi(\mathbf{x}) = -\sqrt{\mu}\varphi(\mathbf{x}), \tag{B5}$$

where $\mu := \lambda^2 + Q\mathbf{C}(\mathbf{x})\mathbf{R}^{-1}\mathbf{C}^T(\mathbf{x})$. We examine the effect of a misrepresentation of the eigenfunction:

$$\hat{\varphi}(\mathbf{x}) := \varphi(\mathbf{x}) + \varepsilon\psi(\mathbf{x}) \tag{B6}$$

where $\varepsilon\psi(\mathbf{x})$ is the discrepancy to the true eigenfunction $\varphi(\mathbf{x})$ with small ε. The dynamics of $\hat{\varphi}(\mathbf{x})$ are given in a factorized representation by

$$\begin{aligned}\dot{\hat{\varphi}}(\mathbf{x}) = \dot{\varphi}(\mathbf{x}) + \varepsilon\dot{\psi}(\mathbf{x}) &= \lambda\varphi(\mathbf{x}) + \mathbf{C}(\mathbf{x})\mathbf{u} + \varepsilon\nabla\psi\cdot(\mathbf{f}(\mathbf{x}) + \mathbf{B}(\mathbf{x})\mathbf{u}) \\ &= \frac{\lambda\varphi(\mathbf{x}) + \varepsilon\nabla\psi(\mathbf{x})\cdot\mathbf{f}(\mathbf{x})}{\varphi(\mathbf{x}) + \varepsilon\psi(\mathbf{x})}\hat{\varphi}(\mathbf{x}) + (\mathbf{C}(\mathbf{x}) + \varepsilon\mathbf{D}(\mathbf{x}))\,\mathbf{u}\end{aligned} \tag{B7}$$

with $\mathbf{D}(\mathbf{x}) := \nabla\psi(\mathbf{x})\cdot\mathbf{B}(\mathbf{x})$. The upper bound for the error in μ due to the misrepresentation of $\varphi(\mathbf{x})$ is

$$\begin{aligned}|\mu - \hat{\mu}| &= \left|\lambda^2 + Q\mathbf{C}(\mathbf{x})\mathbf{R}^{-1}\mathbf{C}^T(\mathbf{x}) - \left(\frac{\lambda\varphi(\mathbf{x}) + \varepsilon\nabla\psi(\mathbf{x})\cdot\mathbf{f}(\mathbf{x})}{\varphi(\mathbf{x}) + \varepsilon\psi(\mathbf{x})}\right)^2 - Q(\mathbf{C}(\mathbf{x}) + \varepsilon\mathbf{D}(\mathbf{x}))\mathbf{R}^{-1}(\mathbf{C}(\mathbf{x}) + \varepsilon\mathbf{D}(\mathbf{x}))^T\right| \\ &= \left|\lambda^2 - \varepsilon Q(\mathbf{C}\mathbf{R}^{-1}\mathbf{D}^T + \mathbf{D}\mathbf{R}^{-1}\mathbf{C}^T) - \varepsilon^2 Q\mathbf{D}\mathbf{R}^{-1}\mathbf{D}^T - \frac{\lambda^2\varphi^2 + \varepsilon 2\lambda\varphi\nabla\psi\cdot\mathbf{f} + \varepsilon^2(\nabla\psi\cdot\mathbf{f})^2}{(\varphi + \varepsilon\psi)^2}\right| \\ &\leqslant \left|\lambda^2 - \varepsilon Q(\mathbf{C}\mathbf{R}^{-1}\mathbf{D}^T + \mathbf{D}\mathbf{R}^{-1}\mathbf{C}^T) - \varepsilon^2 Q\mathbf{D}\mathbf{R}^{-1}\mathbf{D}^T - \frac{\lambda^2\varphi^2 + \varepsilon 2\lambda\varphi\nabla\psi\cdot\mathbf{f} + \varepsilon^2(\nabla\psi\cdot\mathbf{f})^2}{\varphi^2(\mathbf{x})}\right| \\ &= \left|-\varepsilon Q(\mathbf{C}\mathbf{R}^{-1}\mathbf{D}^T + \mathbf{D}\mathbf{R}^{-1}\mathbf{C}^T) - \varepsilon^2 Q\mathbf{D}\mathbf{R}^{-1}\mathbf{D}^T - \frac{\varepsilon 2\lambda\varphi\nabla\psi\cdot\mathbf{f} + \varepsilon^2(\nabla\psi\cdot\mathbf{f})^2}{\varphi^2}\right| \\ &= \left|-\varepsilon\left(Q\mathbf{C}\mathbf{R}^{-1}\mathbf{D}^T + Q\mathbf{D}\mathbf{R}^{-1}\mathbf{C}^T + 2\lambda\frac{\nabla\psi\cdot\mathbf{f}}{\varphi(\mathbf{x})}\right) - \varepsilon^2\left(Q\mathbf{D}\mathbf{R}^{-1}\mathbf{D}^T + \frac{(\nabla\psi\cdot\mathbf{f})^2}{\varphi^2(\mathbf{x})}\right)\right|.\end{aligned} \tag{B8}$$

Appendix C. Series solutions for eigenfunctions

It is possible to solve the PDE in (37) for eigenfunctions using standard techniques, such as Taylor or Laurent series.

C.1. Linear dynamics

Consider linear dynamics

$$\frac{\mathrm{d}}{\mathrm{d}t}x = x. \tag{C1}$$

Assuming a Taylor series expansion for $\varphi(x)$:

$$\varphi(x) = c_0 + c_1 x + c_2 x^2 + c_3 x^3 + \cdots$$

then the gradient and directional derivatives are given by:

$$\nabla\varphi = c_1 + 2c_2x + 3c_3x^2 + 4c_4x^3 + \cdots$$
$$\nabla\varphi\cdot f = c_1x + 2c_2x^2 + 3c_3x^3 + 4c_4x^4 + \cdots$$

Solving for terms in (37), $c_1 = 0$ must hold. For any positive integer λ, only one coefficient may be nonzero. Specifically, for $\lambda = k \in \mathbb{Z}^+$, then $\varphi(x) = cx^k$ is an eigenfunction for any constant c. For instance, if $\lambda = 1$, then $\varphi(x) = x$.

C.2. Quadratic nonlinear dynamics

Consider a nonlinear dynamical system

$$\frac{\mathrm{d}}{\mathrm{d}t}x = x^2. \tag{C2}$$

There is no Taylor series that satisfies (37), except the trivial solution $\varphi = 0$ for $\lambda = 0$. Instead, we use a Laurent series:

$$\begin{aligned}\varphi(x) = &\cdots + c_{-3}x^{-3} + c_{-2}x^{-2} + c_{-1}x^{-1} + c_0\\ &+ c_1x + c_2x^2 + c_3x^3 + \cdots.\end{aligned}$$

The gradient and directional derivatives are given by:

$$\begin{aligned}\nabla\varphi = &\cdots - 3c_{-3}x^{-4} - 2c_{-2}x^{-3} - c_{-1}x^{-2} + c_1 + 2c_2x\\ &+ 3c_3x^2 + 4c_4x^3 + \cdots\\ \nabla\varphi\cdot f = &\cdots - 3c_{-3}x^{-2} - 2c_{-2}x^{-1} - c_{-1} + c_1x^2 + 2c_2x^3\\ &+ 3c_3x^4 + 4c_4x^5 + \cdots.\end{aligned}$$

All coefficients with positive index are zero, i.e. $c_k = 0$ for $k \geqslant 1$. The nonpositive index coefficients are given by the recursion $\lambda c_{k+1} = kc_k$, for $k \leqslant -1$. The Laurent series is

$$\varphi(x) = c_0\left(1 - \lambda x^{-1} + \frac{\lambda^2}{2}x^{-2} - \frac{\lambda^3}{3!}x^{-3} + \cdots\right) = c_0e^{-\lambda/x}.$$

This holds for all $\lambda \in \mathbb{C}$. There are also other Koopman eigenfunctions that can be identified from the series.

C.3. Polynomial nonlinear dynamics

For a more general nonlinear dynamical system

$$\frac{\mathrm{d}}{\mathrm{d}t}x = ax^n, \tag{C3}$$

$\varphi(x) = e^{\frac{\lambda}{(1-n)a}x^{1-n}}$ is an eigenfunction for all $\lambda \in \mathbb{C}$.

ORCID iDs

Eurika Kaiser https://orcid.org/0000-0001-6049-0812
J Nathan Kutz https://orcid.org/0000-0002-6004-2275
Steven L Brunton https://orcid.org/0000-0002-6565-5118

References

[1] Abraham I, De La Torre G and Murphey T D 2017 Model-based control using Koopman operators (arXiv:1709.01568)
[2] Allgöwer F, Badgwell T A, Qin J S, Rawlings J B and Wright S J 1999 Nonlinear predictive control and moving horizon estimation: an introductory overview *Advances in Control* (Berlin: Springer) pp 391–449
[3] Allgöwer F, Findeisen R and Nagy Z K 2004 Nonlinear model predictive control: from theory to application *J. Chin. Inst. Chem. Eng.* **35** 299–315
[4] Arbabi H, Korda M and Mezić I 2019 A data-driven Koopman model predictive control framework for nonlinear partial differential equations *Proc. Conf. on Decision and Control* (IEEE) pp 6409–14
[5] Arbabi H and Mezić I 2016 Ergodic theory, dynamic mode decomposition and computation of spectral properties of the Koopman operator (arXiv:1611.06664)
[6] Ariyur K B and Krstić M 2003 *Real-Time Optimization by Extremum-Seeking Control* (New York: Wiley)
[7] Aström K J and Furuta K 2000 Swinging up a pendulum by energy control *Automatica* **36** 287–95
[8] Bagheri S 2013 Koopman-mode decomposition of the cylinder wake *J. Fluid Mech.* **726** 596–623
[9] Bamieh B and Giarré L 2002 Identification of linear parameter varying models *Int. J. Robust Nonlinear Control* **12** 841–53

[10] Banks S P 1992 Infinite-dimensional Carleman linearization, the Lie series and optimal control of non-linear partial differential equations *Int. J. Syst. Sci.* **23** 663–75

[11] Beeler S C and Cox D E 2004 State-dependent Riccati equation regulation of systems with state and control nonlinearities NASA/CR-2004-213245

[12] Bellman R and Kalaba R 1964 *Selected Papers on Mathematical Trends in Control Theory* (New York: Dover)

[13] Bellman R E 1957 *Dynamic Programming* (Princeton, NJ: Princeton University Press)

[14] Berger E, Sastuba M, Vogt D, Jung B and Amor H B 2015 Estimation of perturbations in robotic behavior using dynamic mode decomposition *J. Adv. Robot.* **29** 331–43

[15] Bertsekas D P 2005 *Dynamic Programming and Optimal Control* (Belmont, MA: Athena Scientific)

[16] Billings S A 2013 *Nonlinear System Identification: Narmax Methods in the Time, Frequency and Spatio-Temporal Domains* (New York: Wiley)

[17] Brockett R W 1976 Volterra series and geometric control theory *Automatica* **12** 167–76

[18] Brunton B W, Johnson L A, Ojemann J G and Kutz J N 2016 Extracting spatial–temporal coherent patterns in large-scale neural recordings using dynamic mode decomposition *J. Neurosci. Methods* **258** 1–15

[19] Brunton S L, Brunton B W, Proctor J L, Kaiser E and Kutz J N 2017 Chaos as an intermittently forced linear system *Nat. Commun.* **8** 19

[20] Brunton S L, Brunton B W, Proctor J L and Kutz J 2016 Koopman invariant subspaces and finite linear representations of nonlinear dynamical systems for control *PLoS One* **11** e0150171

[21] Brunton S L and Noack B R 2015 Closed-loop turbulence control: progress and challenges *Appl. Mech. Rev.* **67** 050801-1–48

[22] Brunton S L, Proctor J L and Kutz J N 2016 Discovering governing equations from data by sparse identification of nonlinear dynamical systems *Proc. Natl Acad. Sci* **113** 3932–7

[23] Brunton S L, Proctor J L, Tu J H and Kutz J N 2015 Compressed sensing and dynamic mode decomposition *J. Comp. Dyn.* **2** 165–91

[24] Budišić M and Mezić I 2012 Geometry of the ergodic quotient reveals coherent structures in flows *Physica* D **241** 1255–69

[25] Budišić M, Mohr R and Mezić I 2012 Applied Koopmanism *Chaos* **22** 047510

[26] Camacho E F and Alba C B 2007 *Model Predictive Control* 2nd edn Advanced textbooks in control and signal processing (London: Springer)

[27] Charlet B, Lévine J and Marino R 1989 On dynamic feedback linearization *Syst. Control Lett.* **13** 143–51

[28] Chartrand R 2011 Numerical differentiation of noisy, nonsmooth data *ISRN Appl. Math.* **2011** 164564

[29] Cimen T 2008 State-dependent Riccati equation (SDRE) control: a survey *IFAC Proc. Volumes* **41** 3761–75

[30] Cloutier J, D'Souza C and Mracek C 1996 Nonlinear regulation and nonlinear h_∞ control via the state-dependent Riccati equation technique: part 1, theory; part 2, examples *Proc. First Int. Conf. on Nonlinear Problems in Aviation and Aerospace, Daytona Beach, FL* pp 117–41

[31] Cloutier J R 1997 State-dependent Riccati equation techniques: an overview *Proc. American Conf.* vol 2 (IEEE) pp 932–6 (https://www.osti.gov/biblio/481985)

[32] Das S and Giannakis D 2019 Delay-coordinate maps and the spectra of Koopman operators *J. Stat. Phys.* **175** 1107–45

[33] Dawson S T M, Hemati M S, Williams M O and Rowley C W 2016 Characterizing and correcting for the effect of sensor noise in the dynamic mode decomposition *Exp. Fluids* **57** 1–19

[34] Dellnitz M, Froyland G and Junge O 2001 The algorithms behind GAIO—set oriented numerical methods for dynamical systems *Ergodic Theory, Analysis and Efficient Simulation of Dynamical Systems* (Berlin: Springer) pp 145–74

[35] Dellnitz M and Junge O 2002 Set oriented numerical methods for dynamical systems *Handbook of Dynamical Systems* vol 2 Fiedler B (Amsterdam: Elsevier) pp 221–64

[36] Dullerud G E and Paganini F 2000 A course in robust control theory: a convex approach *Texts in Applied Mathematics* (Berlin: Springer)

[37] Edwards C and Spurgeon S 1998 *Sliding Mode Control: Theory and Applications* (Boca Raton, FL: CRC Press)

[38] Efron B, Hastie T, Johnstone I and Tibshirani R 2004 Least angle regression *Ann. Stat.* **32** 407–99

[39] Eren U, Prach A, Koçer B B, Raković S V, Kayacan E and Açıkmeşe B 2017 Model predictive control in aerospace systems: current state and opportunities *J. Guid. Control Dyn.* **40** 1541–66

[40] Erichson N B, Brunton S L and Kutz J N 2016 Compressed dynamic mode decomposition for real-time object detection *J. Real-Time Image Proc.* **16** 1479–92

[41] Froyland G 2013 An analytic framework for identifying finite-time coherent sets in time-dependent dynamical systems *Physica* D **250** 1–19

[42] Giannakis D 2019 Data-driven spectral decomposition and forecasting of ergodic dynamical systems *Appl. Comput. Harmon. Anal.* **47** 338–96

[43] Grilli M, Schmid P J, Hickel S and Adams N A 2012 Analysis of unsteady behaviour in shockwave turbulent boundary layer interaction *J. Fluid Mech.* **700** 16–28

[44] Grosek J and Kutz J N 2014 Dynamic mode decomposition for real-time background/foreground separation in video (arXiv:1404.7592)

[45] Guckenheimer J and Holmes P 1983 Nonlinear oscillations, dynamical systems and bifurcations of vector fields *Applied Mathematical Sciences* vol 42 (Berlin: Springer)

[46] Gueniat F, Mathelin L and Pastur L 2015 A dynamic mode decomposition approach for large and arbitrarily sampled systems *Phys. Fluids* **27** 025113

[47] Hansen N, Niederberger A S P, Guzzella L and Koumoutsakos P 2009 A method for handling uncertainty in evolutionary optimization with an application to feedback control of combustion *IEEE Trans. Evol. Comput.* **13** 180–97

[48] Haseli M and Cortés J 2019 Learning Koopman eigenfunctions and invariant subspaces from data: symmetric subspace decomposition (arXiv:1909:01419)

[49] Hemati M and Yao H 2017 Dynamic mode shaping for fluid flow control: new strategies for transient growth suppression *8th AIAA Theoretical Fluid Conf.* vol 3160 (https://doi.org/10.2514/6.2017-3160)

[50] Hemati M S and Rowley C W 2015 De-biasing the dynamic mode decomposition for applied Koopman spectral analysis (arXiv:1502.03854)

[51] Hemati M S, Williams M O and Rowley C W 2014 Dynamic mode decomposition for large and streaming datasets *Phys. Fluids* **26** 111701

[52] Hua J-C, Noorian F, Moss D, Leong P H and Gunaratne G H 2017 High-dimensional time series prediction using kernel-based Koopman mode regression *Nonlinear Dyn.* **90** 1785–806
[53] Isidori A 2013 *Nonlinear Control Systems* (Berlin: Springer)
[54] Graff J, Xu X, Lagor F D and Singh T 2019 Reduced-order modeling using dynamic mode decomposition and least angle regression *Aiaa Aviation Forum (AIAA)* (*17–21 June 2019 Dallas, Texas*) 2019–3072
[55] Jovanović M, Schmid P and Nichols J 2014 Sparsity-promoting dynamic mode decomposition *Phys. Fluids* **26** 024103
[56] Kaiser E, Kutz J and Brunton S 2020 Data-driven approximations of dynamical systems operators for control *Invited Chapter for The Koopman Operator in Systems and Control* (Berlin: Springer) pp 197–234
[57] Kawahara Y 2016 Dynamic mode decomposition with reproducing kernels for Koopman spectral analysis *Advances in Neural Information Processing Systems* vol 29, D Lee, M Sugiyama, U Luxburg, I Guyon and R Garnett (New York: Curran Associates) pp 911–9
[58] Khalil H K 1996 *Noninear Systems* (Englewood Cliffs, NJ: Prentice-Hall)
[59] Klus S, Koltai P and Schütte C 2016 On the numerical approximation of the Perron-Frobenius and Koopman operator *J. Comp. Dyn.* **3** 51–79
[60] Klus S, Nüske F, Peitz S, Niemann J-H, Clementi C and Schütte C 2019 Data-driven approximation of the Koopman generator: model reduction, system identification, and control (arXiv:1909:10638v2)
[61] Kokotovic P V 1992 The joy of feedback: nonlinear and adaptive *IEEE Control syst.* **12** 7–17
[62] Kokotovic P V, O'malley R E and Sannuti P 1976 Singular perturbations and order reduction in control theory—an overview *Automatica* **12** 123–32
[63] Koopman B O 1931 Hamiltonian systems and transformation in Hilbert space *Proc. Natl Acad. Sci* **17** 315–8
[64] Korda M and Mezić I 2016 Linear predictors for nonlinear dynamical systems: Koopman operator meets model predictive control (arXiv:1611.03537)
[65] Korda M and Mezić I 2020 Optimal construction of Koopman eigenfunctions for prediction and control *IEEE Trans. Autom. Control* **1** 1
[66] Kowalski K, Steeb W-H and Kowalksi K 1991 *Nonlinear Dynamical Systems and Carleman Linearization* (Singapore: World Scientific)
[67] Krstić M, Kanellakopoulos I and Kokotović P V 1995 *Nonlinear and Adaptive Control Design* (New York: Wiley)
[68] Kutz J N, Brunton S L, Brunton B W and Proctor J L 2016 *Dynamic Mode Decomposition: Data-Driven Modeling of Complex Systems* (Philadelphia, PA: SIAM)
[69] Kutz J N, Fu X and Brunton S L 2016 Multi-resolution dynamic mode decomposition *SIAM J. Appl. Dyn. Syst.* **15** 713–35
[70] Kutz J N, Grosek J and Brunton S L 2016 Dynamic mode decomposition for robust PCA with applications to foreground/background subtraction in video streams and multi-resolution analysis *CRC Handbook of Robust Low-Rank and Sparse Matrix Decomposition: Applications in Image and Video Processing* 1st edn, ed T Bouwmans, Aybat N S and Zahzah E (New York: Chapman and Hall/CRC) (https://doi.org/10.1201/b20190-31)
[71] Lan Y and Mezić I 2013 Linearization in the large of nonlinear systems and Koopman operator spectrum *Physica* D **242** 42–53
[72] Ljung L 1999 *System Identification: Theory for the User* (Engiewood Cliffs, NJ: Prentice Hall)
[73] Lusch B, Kutz J N and Brunton S L 2018 Deep learning for universal linear embeddings of nonlinear dynamics *Nat. Commun.* **9** 4950
[74] Mangan N M, Brunton S L, Proctor J L and Kutz J N 2016 Inferring biological networks by sparse identification of nonlinear dynamics *IEEE Trans. Mol. Biol. Multi-Scale Commun.* **2** 52–63
[75] Mauroy A and Goncalves J 2016 Linear identification of nonlinear systems: a lifting technique based on the Koopman operator (*Conf. Decision and Control (CDC)*) pp 6500–5
[76] Mauroy A and Mezic I 2013 A spectral operator-theoretic framework for global stability (*Decision and Control (CDC), 2013 IEEE 52nd Conf. on*) (IEEE) pp 5234–9
[77] Mauroy A and Mezić I 2016 Global stability analysis using the eigenfunctions of the Koopman operator *IEEE Trans. Autom. Control* **61** 3356–69
[78] Mayne D Q, Rawlings J B, Rao C V and Scokaert P O M 2000 Constrained model predictive control: stability and optimality *Automatica* **36** 789–814
[79] Mezić I 2005 Spectral properties of dynamical systems, model reduction and decompositions *Nonlinear Dyn.* **41** 309–25
[80] Mezić I 2013 Analysis of fluid flows via spectral properties of the Koopman operator *Ann. Rev. Fluid Mech.* **45** 357–78
[81] Mezić I 2015 On applications of the spectral theory of the Koopman operator in dynamical systems and control theory (*Conf. Decision and Control (CDC)*) (IEEE) pp 7034–41
[82] Mezic I 2017 Koopman operator spectrum and data analysis (arXiv:1702.07597)
[83] Mezić I 2017 *Spectral Operator Methods in Dynamical Systems: Theory and Applications* (Berlin: Springer)
[84] Mezić I and Banaszuk A 2004 Comparison of systems with complex behavior *Physica* D **197** 101–33
[85] Nelles O 2013 *Nonlinear System Identification: From Classical Approaches to Neural Networks and Fuzzy Models* (Berlin: Springer)
[86] Noé F and Nuske F 2013 A variational approach to modeling slow processes in stochastic dynamical systems *Multiscale Model. Simul.* **11** 635–55
[87] Nüske F, Schneider R, Vitalini F and Noé F 2016 Variational tensor approach for approximating the rare-event kinetics of macromolecular systems *J. Chem. Phys.* **144** 054105
[88] Pan S, Arnold-Medabalimi N and Duraisamy K 2020 Sparsity-promoting algorithms for the discovery of informative koopman invariant subspaces (arXiv:2002:10637)
[89] Pearson J D 1962 Approximation methods in optimal control i. Sub-optimal control *Int. J. Electron.* **13** 453–69
[90] Peng H, Wu J, Inoussa G, Deng Q and Nakano K 2009 Nonlinear system modeling and predictive control using the RBF nets-based quasi-linear ARX model *Control Eng. Pract.* **17** 59–66
[91] Pontryagin L, Boltyanskii V, Gamkrelidze R and Mishchenko E 1962 *The Mathematical Theory of Optimal Processes* (New York: Interscience Publishers)
[92] Proctor J L, Brunton S L and Kutz J N 2016 Dynamic mode decomposition with control *SIAM J. Appl. Dyn. Sys.* **15** 142–61
[93] Proctor J L, Brunton S L and Kutz J N 2018 Generalizing Koopman theory to allow for inputs and control *SIAM J. Appl. Dyn. Syst.* **17** 909–30
[94] Proctor J L and Eckhoff P A 2015 Discovering dynamic patterns from infectious disease data using dynamic mode decomposition *Int. Health* **7** 139–45

[95] Qu Q, Sun J and Wright J 2014 Finding a sparse vector in a subspace: linear sparsity using alternating directions *Adv. Neural Inform. Process. Syst.* **27** 3401–9
[96] Rowley C W, Mezić I, Bagheri S, Schlatter P and Henningson D 2009 Spectral analysis of nonlinear flows *J. Fluid Mech.* **645** 115–27
[97] Rugh W J and Shamma J S 2000 Research on gain scheduling *Automatica* **36** 1401–25
[98] Santosa F and Symes W W 1986 Linear inversion of band-limited reflection seismograms *SIAM J. Sci. Stat. Comput.* **7** 1307–30
[99] Sastry S S 2013 *Nonlinear Systems: Analysis, Stability and Control* vol 10 (Berlin: Springer)
[100] Schmid P J 2010 Dynamic mode decomposition of numerical and experimental data *J. Fluid Mech.* **656** 5–28
[101] Schmid P J 2011 Application of the dynamic mode decomposition to experimental data *Exp. Fluids* **50** 1123–30
[102] Shadden S, Lekien F and Marsden J 2005 Definition and properties of Lagrangian coherent structures from finite-time Lyapunov exponents in two-dimensional aperiodic flows *Physica* D **212** 271–304
[103] Skogestad S and Postlethwaite I 2005 *Multivariable Feedback Control: Analysis and Design* 2nd edn (New York: Wiley)
[104] Solomon T H and Gollub J P 1988 Chaotic particle transport in time-dependent Rayleigh–Bénard convection *Phys. Rev.* A **38** 6280–6
[105] Sootla A Mauroy A and Ernst D 2017 An optimal control formulation of pulse-based control using Koopman operator (arXiv:1707.08462)
[106] Stengel R F 2012 *Optimal control and estimation* Dover Books on Mathematics (New York: Courier Corporation)
[107] Surana A 2016 Koopman operator based observer synthesis for control-affine nonlinear systems (*55th Conf. Decision and Control (CDC)*) pp 6492–9
[108] Surana A and Banaszuk A 2016 Linear observer synthesis for nonlinear systems using Koopman operator framework *IFAC-PapersOnLine* **49** 716–23
[109] Susuki Y and Mezić I 2015 A prony approximation of Koopman mode decomposition (*Conf. Decision and Control (CDC)*) pp 7022–7
[110] Sutton R S and Barto A G 1998 *Reinforcement Learning: An Introduction* (Cambridge, MA: MIT Press)
[111] Svoronos S A, Papageorgiou D and Tsiligiannis C 1994 Discretization of nonlinear control systems via the Carleman linearization *Chem. Eng. Sci.* **49** 3263–7
[112] Tibshirani R 1996 Regression shrinkage and selection via the lasso *J. R. Stat. Soc.* B **58** 267–88
[113] Tu J H, Rowley C W, Kutz J N and Shang J K 2014 Spectral analysis of fluid flows using sub-Nyquist-rate PIV data *Exp. Fluids* **55** 1–13
[114] Tu J H, Rowley C W, Luchtenburg D M, Brunton S L and Kutz J N 2014 On dynamic mode decomposition: theory and applications *J. Comp. Dyn.* **1** 391–421
[115] Vander Velde W E 1968 *Multiple-Input Describing Functions and Nonlinear System Design* (New York: McGraw-Hill)
[116] Williams M O, Hemati M S, Dawson S T M, Kevrekidis I G and Rowley C W 2016 Extending data-driven Koopman analysis to actuated systems *IFAC-PapersOnLine* **49** 704–9
[117] Williams M O, Kevrekidis I G and Rowley C W 2015 A data-driven approximation of the Koopman operator: extending dynamic mode decomposition *J. Nonlin. Sci.* **25** 1307–46
[118] Williams M O, Rowley C W and Kevrekidis I G 2015 A kernel approach to data-driven Koopman spectral analysis *J. Comp. Dyn.* **2** 247–65
[119] Wilson D and Moehlis J 2014 An energy-optimal methodology for synchronization of excitable media *SIAM J. Appl. Dyn. Sys.* **13** 944–57
[120] Zhang T, Kahn G, Levine S and Abbeel P 2016 Learning deep control policies for autonomous aerial vehicles with MPC-guided policy search *IEEE Int. Conf. Robotics and Automation* pp 528–35